Additive manufacturing of self-healing polymers for soft robotics applications

Ellen Roels

Master thesis submitted under the supervision of
prof. dr. ir. Bram Vanderborght

The co-supervision of
prof. dr. ir. Guy Van Assche

Academic year
2017-2018

In order to be awarded the Masters Degree in
Mechanical engineering option Mechatronics-Construction

In theory, theory and practice are the same.
In practice, they are not.

Contents

Abstract IX

Acknowledgement XI

List of Figures XIII

List of Tables XVI

Acronyms XIX

Motivation 1

1 Introduction 3
- 1.1 Soft robotics 3
- 1.2 Self-healing materials 5
- 1.3 Manufacturing of soft robots 7
  - 1.3.1 Manufacturing techniques for self-healing Diels-Alder materials 7
  - 1.3.2 Additive manufacturing 8
- 1.4 Project goals 11
- 1.5 Outline 12

2 Materials and methods 13
- 2.1 Materials 13
  - 2.1.1 Chemical structure 13
  - 2.1.2 Synthesis 14
  - 2.1.3 Mechanical properties 14
  - 2.1.4 Recycling 16
  - 2.1.5 3D-printing 16
- 2.2 Methods 16
  - 2.2.1 Dynamic Mechanical Analysis 16
  - 2.2.2 Dynamic rheometry 18
  - 2.2.3 Thermogravimetric analysis 18
  - 2.2.4 Differential Scanning Calorimetry 19
  - 2.2.5 Kinetic simulations 19
- 2.3 Characterisation 21
  - 2.3.1 Thermogravimetric analysis 21
  - 2.3.2 Dynamic Mechanical Analysis 21
  - 2.3.3 Rheometry 22

2.4 Conclusion . . . 24

3 Filament extrusion 25
3.1 Initial tests . . . 26
3.2 Simulation of the pre-heating procedure . . . 27
3.3 Failure phenomena . . . 29
3.3.1 Stress relaxation . . . 29
3.3.2 Die swell . . . 29
3.3.3 Sharkskin . . . 29
3.4 Solutions . . . 30
3.4.1 Extrusion speed . . . 30
3.4.2 Die design . . . 30
3.4.3 Drawdown . . . 31
3.4.4 Grinding . . . 32
3.5 Recycling . . . 34
3.6 Results of the filament extrusion . . . 34

4 3D-printing of self-healing polymers 37
4.1 Selection of a 3D-printer . . . 37
4.2 Simulation of the printing process . . . 40
4.2.1 Printing temperature . . . 40
4.2.2 Heated bed - heated environment . . . 42
4.3 Practical 3D-printing . . . 45
4.3.1 Feeding the filament . . . 45
4.3.2 Temperature settings . . . 46
4.4 Print quality . . . 47
4.4.1 Dimensional accuracy . . . 48
4.4.2 Surface finish . . . 48
4.5 Material properties . . . 49
4.5.1 Isotropy . . . 50
4.6 Conclusion . . . 52

5 Towards multi-material printing 53
5.1 Study of the interface between JT5000 and JD4000 . . . 53
5.2 Developing the process for other Diels-Alder materials . . . 54
5.3 Conclusion . . . 55

6 Conclusion and future work 57
6.1 Conclusion . . . 57
6.2 Future work . . . 58

Bibliography 59

Appendices 63

A Synthesis reaction of the Diels-Alder material 65

B Adaptations to the filament extruder 69

C Printer settings 71

D Isotropic tensile tests **73**

E Stress-strain curves of joined samples JT5000-JD4000 **75**

Additive manufacturing of self-healing polymers for soft robotics applications

Master of Science in Electromechanical Engineering
option Mechatronics-Construction

2017-2018

Ellen Roels

Keywords: Additive manufacturing, self-healing polymers, soft robotics, Diels-Alder reaction, 3D-printing

Abstract

With nature as their main source of inspiration, soft robotics is a fast growing field of research. Their inherent softness and flexibility allows for safe interaction with their environment, but makes them also fragile. Whereas traditional (soft) robots are unable to repair themselves after damage, new research in the field of self-healing polymers for soft robotics shows promising results. Self-healing robotic actuators have been successfully developed using elastomeric polymer networks based on thermoreversible Diels-Alder bonds. Up until now, these self-healing actuators are manufactured using a process called shaping-through-folding-and-self-healing, which is labour intensive and limits the design options. In this thesis, a proof of concept for additive manufacturing of self-healing elastomeric polymers is presented. In this work, Fused Filament Fabrication, also known as 3D-printing, is considered. For the development of this process, a first step is to obtain filament for the 3D-printer. This is accomplished by an extrusion process that is optimized specifically for the Diels-Alder networks. The optimization exists of finding several parameters and overcoming the observed failure phenomena. The second step is the 3D-printing itself, which strongly depends on the quality of the obtained filament. This technique was adapted and optimized to make 3D-printing of flexible Diels-Alder elastomers possible. The material was successfully printed and it was proven through experimental verification that the mechanical and chemical properties of the material remain equal before and after the filament extrusion and printing process. However, some limitations remain in the printing process, such as printing overhang, due to the chemical nature of the material. The self-healing properties show also their benefit on the quality of the print: due to the healing, the layer marks that are typical for 3D-printed parts disappear and the parts are airtight. This allowed to print several proofs of concept for soft robotic actuators. 3D-printing of the self-healing actuators allows for a wider range of designs, faster prototyping, and the use of multiple self-healing materials with different mechanical properties within the same design. In addition, the Diels-Alder elastomer networks have the advantage of being completely recyclable, a property used and illustrated throughout this thesis.

Acknowledgement

First and foremost, I would like to express my gratitude towards my promotor prof. dr. ir. Bram Vanderborght, co-promotor prof. dr. ir. Guy Van Assche, and advisor ir. Seppe Terryn for their guidance and support during this research. The door to their offices was always open and they were always available to discuss questions, problems and ideas. Thank you for giving me the opportunity to join this interdisciplinary team and research this very interesting topic.

Besides them, special thanks goes towards the research groups FYSC and R&MM for the fun times in the lab, and specifically to Joost and Robrecht for their insights and help on the chemical side of this thesis, as I originally lacked background therein.

I would also like to thank my family and friends for their mental support and patience the previous five years, especially my parents Monique and Hubert, boyfriend Ruben, and friends Pieter-Jan and Thomas. Thank you for all the fantastic moments we shared, the hilarious quotes, the laughs and giggles, but also the burden of long days in the lab and stressful exams.

Ellen

List of Figures

1.1 Soft grippers commercially available. The link with biology is obvious in the OctopusGripper in (a). Both are able to easily grab and hold fragile objects with an irregular form, whereas hard grippers are rather unable to achieve this behaviour without the need of extensive control. [Source:1.1a-`festo.com`, 1.1b - `empirerobotics.com`] 4
1.2 Different self-healing (SH) pneumatic actuators developed at VUB. The inflatable cells are clearly visible in the hand and gripper [1][2]. 5
1.3 Different techniques can be used to manufacture soft robots in different shapes and dimensions. In this thesis, one of the goals is to research the multi-material manufacturing of soft robots using additive manufacturing, this adaptation is put in a dotted black line. Figure adapted from [3]. 8
1.4 Shaping-through-folding-and-self-healing uses a number of local healing cycles to heal folded sides to each other. Local heating can for example be performed using a soldering iron on a low temperature setting. 9
1.5 In Fused Filament Fabrication (FFF), the plastic filament (red) is fed through a small heated nozzle called the hot-end which is situated on the extruder head (black). The extruder moves in a specified pattern, leaving molten material in the required shape. 10

2.1 A Diels-Alder (DA) reaction is an equilibrium reaction between a diene, which has two double bonds, spaced one carbon atom apart, and a dienophile, which has a double bond connected to an electron withdrawing group R_2. The electrons from the double bonds move cyclic and form a cyclohexene. 13
2.2 Three reactants and a radical inhibitor (hydroquinone) are used in the synthesis. The full synthesis reaction is shown in Appendix A. 15
2.3 TGA analysis of JT5000. These TGA results are obtained using the following procedure: 1. Equilibrate at 50 °C; 2. Ramp 10 °C/min to 600 °C; 3. Isothermal for 5 min; 4. Ramp 100 °C/min to 50 °C. 22
2.4 Stress-strain curves of samples JT5000. Three samples were tested at a strain rate of 60 %/min at an ambient temperature of 25 °C . The ultimate tensile strength is 2.0±0.2 MPa at a strain of 144±10 %. The Young's modulus is 7.9±0.4 MPa. . 23
2.5 The Dynamic Mechanical Analysis (DMA) analysis of JT5000 shows a glass transition temperature (T_g) of -47 °C. Measurement performed on a sample of size 8.94×5.55×0.55 mm with an oscillatory strain of 0.2 %, frequency of 1 Hz, static force of 0.01 N, 125 % force tracking, and a temperature ramp of 2.50 °C/min. . . 23
2.6 The rheometric analysis of JT5000 was performed at various angular velocities ranging from 1.99 rad/s to 19.87 rad/s, depicted as different colours. gel temperature (T_{gel}) is determined as 104 °C in degelation and 105 °C in gelation. 24

3.1 The Noztek Touch is a single screw extruder used to produce the filament. It is equipped with two heaters, a fan, and an extrusion motor. 25
3.2 The filament extrusion parameters are important to get right. Different examples of failure phenomena are shown. (a) Too low temperature. (b) Sharkskin. (c) Diameter variation. 26
3.3 The kinetics of JT5000 are simulated: after 24 hours at room temperature (not shown), the conversion of endo-adduct is 0.63 and for exo-adduct, the conversion is 0.20. Then the temperature is raised to 120 °C for 20 minutes and cooled down again to room temperature where it is left to rest for another 4 hours. At this moment, the conversion of both endo- and exo-adduct is 0.30. 28
3.4 Evolution in the die design from left to right. The newer dies have an increased land length and smaller angle of entrance. 31
3.5 The DA material is brought to below its $\mathrm{T_g}$ by using liquid nitrogen and then grinded to produce fine particles. 32
3.6 Differential Scanning Calorimetry (DSC) analysis of a sample grinded material compared with a reference shows that the grinding operation does not have any influence. Sample mass: 21.09 mg for the grinded sample and 22.45 mg for the reference sample. 33
3.7 DMA analysis of a grinded sample JT5000 (10.6 mm×5.9 mm×1.2 mm) compared with a reference sample (9.4 mm×6.1 mm×1.2 mm) shows a $\mathrm{T_g}$ of −46 °C. Measurement performed with an oscillatory strain of 0.5 %, static force of 0.01 N, 125 % force tracking, and a temperature ramp of 2.50 °C/min. 33
3.8 Bad filament or failed prints can easily be recycled in a four-step cycle. 1. Remould the material in a sheet by heating it up above the $\mathrm{T_{gel}}$. 2. Cut the sheet in small cubes. 3. Feed the cubes in the extruder machine. 4. Extrude new filament. 34
3.9 A batch of filament produced during the filament optimization process. Sharkskin is still present but the general diameter variations in the bulk of the material are good. 35

4.1 Two printers that fulfil the requirements, a detailed comparison is needed in order to decide which one is best for the application. (Source: 4.1a-`shop.prusa3d.com`, 4.1b - `lulzbot.com`) 38
4.2 Graphical illustration of the parameters needed to calculate the heat time t_h. Due to the diameter reduction in the nozzle, the filament velocity v_f is different from the printing velocity v_n. 41
4.3 Simulations of the change in molecular weight during the printing on various temperatures allow to see that the SH material should not be printed below 115 °C. 43
4.4 The heated bed temperature has a large influence on the time to gelation. This time should be as short as possible to prevent the material from flowing. 44
4.5 The time to gelation depends on the printing temperature and the heatbed temperature. Simulation done in steps of 10 s. 44
4.6 Buckling under the metal hobbed gear is to be avoided: the filament gets stuck between the gear and its green plastic housing, which leads to failed prints. . . . 45
4.7 A test specimen of 20 mm×20 mm printed at different extruder temperatures: 117 °C (left), 120 °C (centre), 125 °C (right). A better print quality is achieved at low temperatures. Note that the number of layers printed is not equal in the different samples, due to the filament buckling. The print at 125 °C is above the allowed temperature, but is added for comparison purposes. 47
4.8 A printed sample in JT5000. Almost no texture from the layers is present. 49

4.9 The rheometric analysis of the printed JT5000 was done at various angular velocities ranging from 1.99 rad/s to 19.87 rad/s, depicted as different colours. T_{gel} is determined as 114 °C. 50
4.10 DMA analysis of a printed sample (JT5000) shows a T_g of -52 °C. A reference sample stored under equal conditions shows a T_g of -54 °C. Measurement performed with an oscillatory strain of 0.5 %, static force of 0.01 N, 125 % force tracking, and a temperature ramp of 2.50 °C/min. 51
4.11 Two proofs of concept were printed for soft inflatable elastic robotic actuators. (a) A cell of the gripper and hand as shown in Figure 1.2. (b) A new design for a SH actuator, a sheet on top and below should be added to finalize the design. . . 52

5.1 Microscopic images of the healing of JD4000 (black) and JT5000 (yellow) from left to right. 53
5.2 Filament produced from JT5000 with stoichiometric ratio $r = 0.5$. 55
5.3 A small piece of a multi-material print is successfully obtained. JT5000 (yellow) and JT3000 (blue/green) are printed next to each other. 55

A.1 The three reactants and the radical inhibitor hydroquinone are used in the synthesis. 66
A.2 Combining a Jeffamine with FGE to obtain a furan-functionalized compound. . . 67
A.3 Jx-FGE is combined with DPBM to form a covalent thermoreversible network. . 67

B.1 Schematic drawing of the H-bridge set-up used to control the motor velocity. . . 69

D.1 Stress-strain curves of printed samples JT5000 in the 0 ° direction. Four samples were tested at a strain rate of 60 %/min at an ambient temperature of 25 °C. The ultimate tensile strength is 1.6±0.2 MPa at a strain of 108±21 %. The Young's modulus is 6.2±1.1 MPa. 73
D.2 Stress-strain curves of printed samples JT5000 in the 90 ° direction. Two samples were tested at a strain rate of 60 %/min at an ambient temperature of 25 °C. The ultimate tensile strength is 1.4±0.1 MPa at a strain of 91±34 %. The Young's modulus is 5.3±1.0 MPa. 74
D.3 Stress-strain curves of printed samples JT5000 in the ±45 ° alternating directions. Four samples were tested at a strain rate of 60 %/min at an ambient temperature of 25 °C. The ultimate tensile strength is 1.6±0.2 MPa at a strain of 108±5 %. The Young's modulus is 6.2±0.6 MPa. 74

E.1 Stress-strain curves of samples JD4000 and JT5000 healed to each other for 60 min at 90 °C. Four samples were tested at a strain rate of 60%/min at an ambient temperature of 25 °C with open furnace. The ultimate tensile strength is 1.1±0.1 MPa at a fracture strain of 237±26 %. 75
E.2 Stress-strain curves of samples JD4000 and JT5000 healed to each other for 60 min at 80 °C. Four samples were tested at a strain rate of 60%/min at an ambient temperature of 25 °C with open furnace. The ultimate tensile strength is 1.0±0.3 MPa at a fracture strain of 144±76 %. 76
E.3 Stress-strain curves of samples JD4000 and JT5000 glued to each other. Four samples were tested at a strain rate of 60%/min at an ambient temperature of 25 °C with open furnace. The ultimate tensile strength is 0.3±0.1 MPa at a strain of 43±24 %. 76

List of Tables

2.1 The simulation program uses these parameters to calculate the process kinetics. The pre-exponential factor A is calculated for each reaction using Equation 2.14 by a known value for k at 298.15 K, which are given in this table. 21

3.1 Equal conversion points at various temperatures. 28

4.1 Different printers fulfil the criteria; the Prusa i3 MK2S and the LulzBot TAZ 6 will be looked at in more detail. 39
4.2 Maximum printing velocities at various temperatures. The printing velocities are deduced from the time t_h at which the molecular weight is minimal. The formula $v_n = \frac{l_h \cdot d_f^2}{d_n^2 \cdot t_h}$ is used. 42
4.3 Comparison of the measured mechanical properties in different printing orientations. The detailed measurements are given in Appendix D. 51

5.1 Comparison of the measured mechanical properties at the interface of two DA materials. 54

Acronyms

DA Diels-Alder.

DMA Dynamic Mechanical Analysis.

DPBM 1,1'-(methylenedi-1,4-phenylene)bismaleimide.

DSC Differential Scanning Calorimetry.

FFF Fused Filament Fabrication.

FGE furfuryl glycidyl ether.

SH self-healing.

SLS Selective Laser Sintering.

T_g glass transition temperature.

T_{gel} gel temperature.

T_m melting temperature.

TGA Thermogravimetric analysis.

Motivation

Soft robotics is a fast-emerging field. These soft robots are made out of soft and flexible materials, which makes them considerably safer for interaction with humans and delicate objects (such as fruits). The use of these soft materials also has drawbacks: due to their softness, they are more prone to ruptures or being punctured by sharp objects.

A promising solution to these problems is the use of self-healing (SH) materials. These materials have the property of being able to repair themselves when ruptured. To do this, they need a trigger such as light or heat. At the Vrije Universiteit Brussel, this kind of materials has been researched at the FYSC (Physical Chemistry and Polymer Science) research group for several years now. The materials have been intensively studied and can be synthesized with different mechanical and chemorheological properties.

A cooperative project between the R&MM (Robotics and Multibody Mechanics) research group and FYSC was set up in 2014 by PhD researcher Seppe Terryn in order to study the feasibility of using these materials in soft robots. Several actuators that are able to repair macroscopic damage have been developed [1][2]. One of the problems encountered is the difficult shaping process of these SH polymers. The shaping-by folding-and-self-healing process was developed to produce soft robotic actuators, but this process is time-consuming and the design flexibility is rather limited. Therefore, research is now carried out towards other shaping techniques.

In the FWO-project AMSeR, started in January 2018, Selective Laser Sintering (SLS) will be investigated by the Soft Matter, Rheology and Technology (SMaRT) research group at KULeuven. In parallel, FYSC will explore Fused Filament Fabrication (FFF) of the same SH polymers in this project. Using such a technique allows the manufacturing of more complex parts. It has the potential to be faster, more repeatable, and less labour-intensive.

In this thesis, the different parameters needed for the additive manufacturing of these materials are studied and implemented to print them using FFF. One of the goals is to optimize this process to be able to print soft robotics parts in SH material.

Another problem often encountered in soft robotics, is the interface between two different materials with different mechanical properties. As the developed SH materials can be tuned to have different mechanical properties, while still being able to heal one onto another, these materials can provide a solution to this problem. A 3D-printer equipped with a dual extruder allows to print two different SH materials, and thus more complex actuator designs. During this project, the potential of multi-material extrusion is studied as well.

Chapter 1

Introduction

1.1 Soft robotics

Today, most robots are used in industrial plants. They are very stiff and work in a well defined and structured environment. The typical industrial robot, often referred to as robotic manipulator, still consists of rigid links, actuated by rotational or translational joints. They have a defined number of degrees of freedom, often without any redundancy so that every position with a certain orientation of the end-effector can only be reached in a single way. For most manufacturing or other industrial purposes, this does not pose any problem as the environment is adapted to the robot. These robots are not compliant, they are unable to deviate from their (equilibrium) position by applying an external force such as a human running into them. Therefore, they typically operate inside a cage to prevent humans from coming too close and getting injured.

Typically, this kind of stiff robots does not work well outside of their defined environment. However, there exist a lot of environments that are unstructured and can even be unpredictable, for example, the outside world or the presence of humans. To be able to deploy robots in this kind of environment, compliant robots are being developed. Compliant robots contain flexible elements, such as springs or elastic materials. As a result they can give way when applying an external force [4]. This compliance makes human-robot interaction safer. Imagine a robot that wants to move, following a path for which a human is in the way. A stiff industrial robot with position control would try to follow the path, applying as much force as needed to reach the objective. The human will be hit very hard and will most probably get hurt. A compliant robot will give way and deform around the human by deviating from its equilibrium position. This limits the impact and thus it allows for soft interactions.

Soft robots are also compliant robots and often inspired by biology. They typically consist of soft materials, rather than metals or hard plastics [5][6]. The elasticity modulus of these materials is often close to the ones found in living organisms (10^4-$10^9\,\mathrm{Pa}$) [1]. This opens the possibility for safe interaction with natural environments (such as human interaction) [7]. Moreover, by using soft materials, they are able to deform around obstacles, which makes them very useful for soft grasping applications. They are already finding their way into commercial applications, as described by Bogue [8]. For example, the companies Festo (Figure 1.1a) and Empire Robotics (Figure 1.1b) have soft gripper designs available on the market.

More general, soft actuators can be split into different categories based on actuation modes [3].

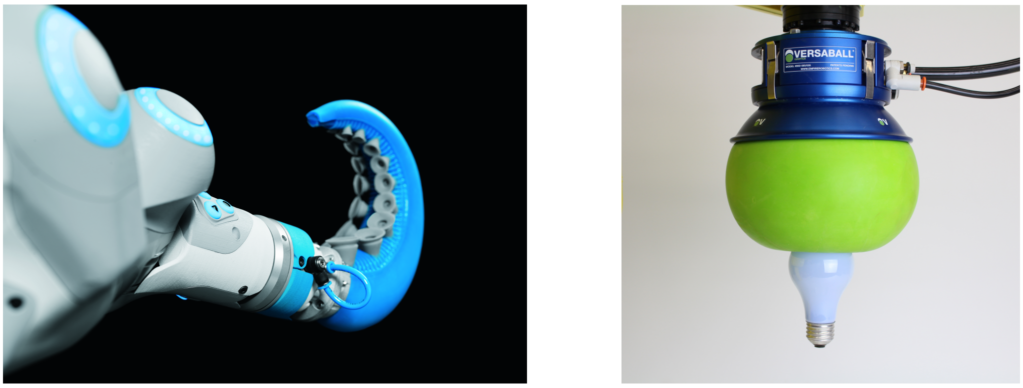

(a) OctopusGripper - Festo **(b)** VERSABALL - Empire Robotics

Figure 1.1: Soft grippers commercially available. The link with biology is obvious in the OctopusGripper in (a). Both are able to easily grab and hold fragile objects with an irregular form, whereas hard grippers are rather unable to achieve this behaviour without the need of extensive control. [Source:1.1a-`festo.com`, 1.1b - `empirerobotics.com`]

Bending actuators are ideal for making grippers, while expanding and contracting actuators are more often used as artificial muscles [9][10][11]. These actuators can either be actuated by tendons connected to a motor ([9][10]) or pneumatically as described by Gorissen et al. [3].

The flexibility and softness of these robotic parts also have several drawbacks. As the used materials are soft and have a low modulus of elasticity, they are more prone to tearing, piercing and other forms of damage, besides the usual wear. This can happen when handling sharp objects or working in an environment with sharp objects or edges. In pneumatically actuated parts, a leak can, for example, happen by applying overpressure in the actuator. When a leak is present in the actuator, it can still work given that the leak is small. However, this will make the actuator less energy efficient and it can apply less force. Because of this behaviour, the trend is to over-dimension (soft) robots, which makes them heavier and more expensive [12]. Moreover, a thicker layer of flexible material will reduce the flexibility. It is clear that the amount of over-dimensioning needed, is preferably as low as possible. Furthermore, permanent deformations can also occur in soft actuators, which are induced by creep. This creep is due to the high stresses acting on the material when creating high pressures inside the actuator [13].

Terryn et al. introduced a method to use self-healing (SH) materials to prevent or limit the over-dimensioning and introduce a recovery possibility after breakdown [1]. A lot of biological systems have SH properties: a wound or broken bone will heal after a certain time without any intervention. Most artificial materials do not have this SH property and most engineering standards are based on failure prevention instead, often using (high) safety factors [14]. This also makes that a lot of robots and other applications are over-dimensioned (especially in task-dynamic environments), which increases overall weight and material costs. If a part does fail, which is even more of a risk in soft robotics (getting cut on sharp objects), the whole -often complex- assembly has to be redone, which is time-consuming and thus expensive.

The use of SH materials makes it possible to heal them in-place when an actuator is rup-

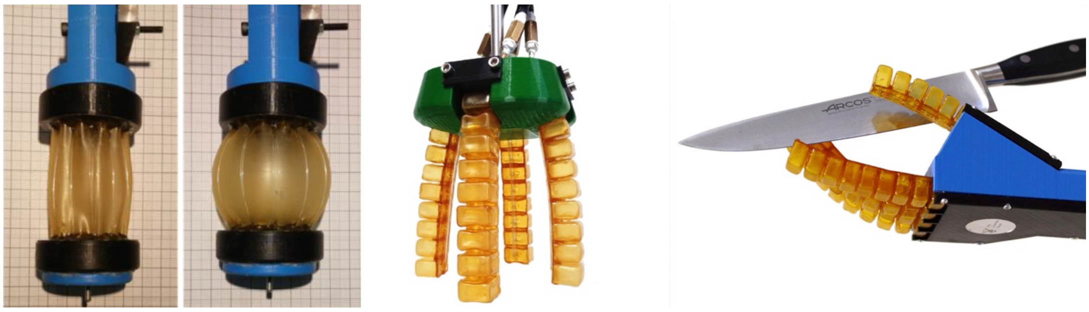
(a) Artificial muscle **(b)** Gripper **(c)** Hand

Figure 1.2: Different SH pneumatic actuators developed at VUB. The inflatable cells are clearly visible in the hand and gripper [1][2].

tured. With this new healing ability, a potential breakdown is only temporary and therefore, less problematic. As a potential breakdown is less of a problem, it is not (or less) necessary to over-dimension the robot. Also for stiff and compliant robots, SH materials can lower the need for over-dimensioning, as illustrated by the SH mechanical fuse developed by Terryn et al. [12]. A mechanical fuse can be used to limit the stress on a tendon: the fuse will break before the tendon breaks. When using a SH fuse, it can be healed instead of replaced. This approach is potentially cheaper than replacing the whole tendon.

Besides the fuse, Terryn et al. already developed a soft hand, gripper, and an artificial muscle [1][2]. As can be seen in Figure 1.2, both the hand and gripper are made of several pneumatic bending actuators. These consist of nine inflatable cells connected to a single pressure source, so that they are inflated equally. When inflating, the cells expand, bending the actuator with the cells facing outwards.

The hand can be used in situations where a safe, direct human-robot interaction is needed, as in assistance robots or rehabilitation devices. The gripper has more applications in industry, where it can be used for handling delicate objects, such as food items. The artificial muscle is based on the Pleated Pneumatic Artifical Muscle, developed by Villegas et al. [11]. When inflated, the folds are pushed outwards, contracting the muscle. Wires inside the folds are used to transfer the tension. The higher the force needed by contraction, the higher the pressure inside the muscle should be, which increases the risk of damage significantly.

1.2 Self-healing materials

Self-healing materials are being researched by institutions around the globe since 2001 [15], i.a. VUB. At the moment of writing, the knowledge and use of SH materials stays mainly in academia, with only limited (coating-based) applications already available on the market. One of the most well known applications is the ‘Scratch Shield’ [16] coating that car manufacturer Nissan uses on several of their cars. Another example is the G Flex smartphone from LG, which has a SH back cover [17].

A whole range of different SH materials exist, with a lot of inherent differences [18]. Although in this thesis only polymers are considered, there exist other SH materials. SH metals are being researched, but only few results are documented. SH ceramics and composites are in a more advanced state of development, with a useful and market-ready application in SH concrete [14]. These SH materials can be split in two categories by looking at the healing mechanism: intrinsic and extrinsic healing.

Intrinsic healing Intrinsic materials have the SH property due to their chemical structure. They have reversible bonds, which can be of different types, such as hydrogen bonds or reversible covalent bonds.

Extrinsic healing Extrinsic materials have capsules with healing agent inside. When the material is cut or scratched, also several capsules are cut, and the healing agent flows out of its capsule where it can heal the material.

One of the disadvantages of extrinsic materials is the limited healing factor: once the capsules are empty, the material will no longer be able to heal. Guimard et al. also state that intrinsic SH materials, and more specifically polymers, can be made with better mechanical properties, making them specifically useful in robotics applications [18]. As the capsules in extrinsic materials need to break, these materials are more brittle than intrinsic materials, rendering them relatively useless in soft robotics.

The classification of SH materials can also be made by looking how the healing is initiated, and again it is possible to describe two categories.

Autonomous systems Autonomous systems do not need an extra stimulus to start healing, the mechanical damage is enough. These materials can be both intrinsic and extrinsic, but in general, most extrinsic materials are autonomous.

Non-autonomous systems Non-autonomous systems need a stimulus to start and continue the healing process, this can, for example be light or heat. The stimulus does not always have to be induced by a human: sometimes the stimulus is present in the working environment, e.g. the ‘Scratch Shield’ coating has its stimulus (heat) present when the car stands or drives in sunlight.

SH materials have been used in a few (soft) robotics applications. Cheng et al. used a wax coated polyurethane to obtain a structure that can be soft when heated and stiff at room temperature. The wax can heal itself by heat addition when it cracks [19].

Also at the VUB research groups R&MM and FYSC, Terryn et al. used polymers to make SH soft robotic parts [1]. These polymers are non-autonomous and intrinsic, the trigger to induce healing is heat. Terryn et al. describe the healing process in five steps.

1. The material is damaged.
2. The damaged part is heated to about 80 °C. This induces the reverse Diels-Alder (DA) reaction and breaks the DA bonds (see Chapter 2).
3. The material remains at this elevated temperature to increase the mobility of the material such that it can fill the cuts and gaps. This takes 20-40 min.
4. The material is cooled again, recovering a fraction of the broken bonds and recreating the network.

5. The material is left to rest at room temperature to fully recover the mechanical properties.

The DA polymers used can be made with various mechanical properties (as elaborated in Section 2.1.1), ranging from very brittle to very soft. A big advantage of these materials is that the whole range of materials can heal to each other, making it possible to have robotic parts made with different kinds of this material.

1.3 Manufacturing of soft robots

Currently, soft robots are manufactured using several techniques; Gorissen et al. describe four processes, as illustrated in Figure 1.3. They also divide bending inflatable soft actuators in different categories based on their principle of asymmetry. At least one type of asymmetry is needed this type of actuator to allow the bending. Multi-material actuators work with a central void, but due to the different Young's modulus of the materials, bending will occur upon inflation. Actuators based on a corrugated void, such as the SH actuators in Figure 1.2b and Figure 1.2c have expanding voids on one side that induce the bending. Finally, an eccentric void can also be used to have a bending actuator, here, the void is placed eccentrically inside the surrounding elastic material.

The different techniques used to manufacture these types of bending actuators are:

3D-moulding A mould is made, at lab scale usually by conventional additive manufacturing techniques to lower the cost and processing time. In this mould, the soft material is injected and be left to cure. Using this technique limits the possible shape of the actuator; complex retracting shapes or voids are impossible as this prevents the mould from being removed. A solution can be to use a complex piecewise mould.

2D-moulding Instead of making a complex actuator design directly, it can be divided in several 2D layers. These layers can be made in separate easier moulds, but have to be joined afterwards. This joining is most often the most critical and difficult part of the process. Advantages of this technique are that is possible to create very complex parts as easily as more simple parts, due to the layering. Another advantage is the possibility to have multi-material actuators, moulding a few layers in other materials is enough.

Full lithography For very small actuators, lithography can be used to etch different layers onto each other using a photolithographic process [20]. This has only been used for very few actuators and is added here for completeness.

Additive manufacturing This process is extensively described in Section 1.3.2. However, Gorissen et al. state that additive manufacturing is currently not used for the manufacturing of multi-material actuators [3]. In this project, one of the goals is to develop a method that allows this multi-material manufacturing.

1.3.1 Manufacturing techniques for self-healing Diels-Alder materials

The current problem with this SH material is the manufacturing of parts. 3D-moulding is impossible with the current material as the solvent that is needed for casting has to be extracted

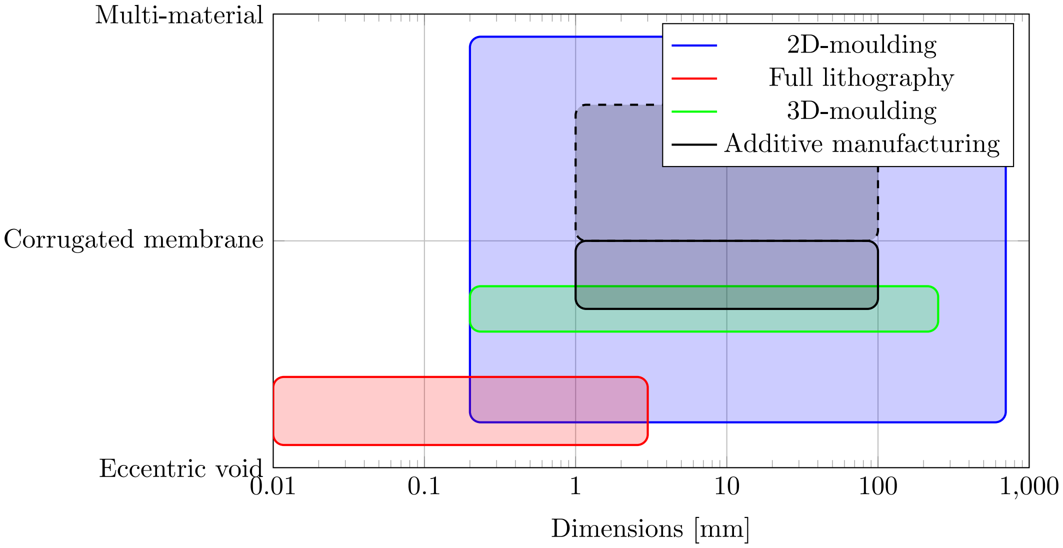

Figure 1.3: Different techniques can be used to manufacture soft robots in different shapes and dimensions. In this thesis, one of the goals is to research the multi-material manufacturing of soft robots using additive manufacturing, this adaptation is put in a dotted black line. Figure adapted from [3].

in order for the material to cure. Also methods using high temperatures are non-ideal, as the material will form irreversible bonds (which reduce the SH property) and at even higher temperatures, degradation can take place.

To overcome this problem, Terryn et al. created a manufacturing technique called ‘shaping-through-folding-and-self-healing’, illustrated in Figure 1.4. The material is produced in sheets and using the SH property after folding, ribs are welded and various shapes are obtained. This process is very slow and labour intensive. A small scale solution lays in the additive manufacturing (3D-printing) of these materials, which will also allow to manfacture more complex shapes.

1.3.2 Additive manufacturing

Additive manufacturing nowadays is a relative cheap and common manufacturing technique [21]. The printing process is slow and takes a few hours even for small parts, but the set-up work and cost is non-existent, compared to for example injection moulding. This makes 3D-printing the process of choice for creating prototypes and iterating designs. Prototypes can be made within the scope of a few hours, making the iteration process a lot faster compared to conventional machining [22]. The technology can also be used for producing small batches efficiently.

There exist several techniques that fall within the category of additive manufacturing.

Selective laser sintering In Selective Laser Sintering (SLS), an object is created by fusing powder together with a laser beam. As in all additive manufacturing techniques, the object is built layer by layer. With SLS, a new layer is built by applying a new layer of material powder on

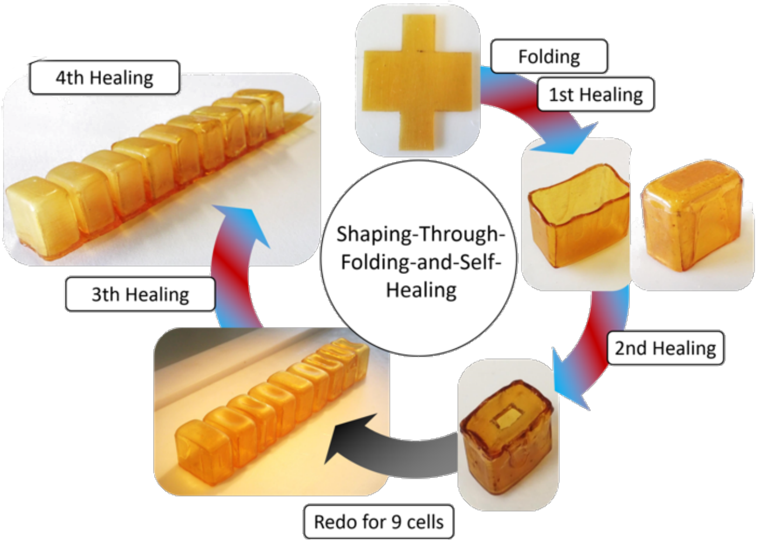

Figure 1.4: Shaping-through-folding-and-self-healing uses a number of local healing cycles to heal folded sides to each other. Local heating can for example be performed using a soldering iron on a low temperature setting.

top of the previous one. A laser then moves over the powder, drawing the shape of the new layer and fusing it together locally by increasing the powder temperature above the glass transition temperature (T_g) or melting temperature (T_m). Examples of widely used materials for SLS are poly-amides (nylon) and thermoplastic polyurethanes.

Stereolithography Stereolithography is comparable with SLS, but instead of the powder, a liquid monomer resin is used, and this is polymerized using a UV light beam rather than a laser. The print bed can move up and down in a bath of this liquid photosensitive resin [20].

Fused filament fabrication Most hobbyist 3D-printers use the Fused Filament Fabrication (FFF) process, which is shown in Figure 1.5. A cylinder with small diameter (often 1.75 mm or 2.85 mm, the latter is also referred to as 3 mm filament), the filament, is extruded through a heated nozzle. The printing head moves in the layer pattern while extruding the filament, depositing a new layer of molten plastic on its way. When the layer is finished, the printing head moves up or the bed moves down (depending on the construction of the printer) so there is space to deposit a new layer of material [20].

During this project, the choice was made to work solely with FFF as it is considered the technique that has the most potential for now. FFF is also known under the term Fused Deposition Modeling (FDM), which was patented by Crump in 1992, so preference is given to the patent-free name FFF [23]. These 3D-printers are mostly optimized to work with hard plastics such as the bioplastic polylactide (PLA, Young's modulus: 3 GPa-16 GPa [24]) or acrylonitrile butadiene styrene (ABS[1], Young's modulus: 2.3 GPa), but there also exist more flexible materials such as the thermoplastic polyurethane NinjaFlex[2] (Young's modulus: 12 MPa). The modulus

---

[1] `http://www.bestech.com.au/wp-content/uploads/Modulus-of-Elasticity.pdf`, accessed 27/08/2017

[2] `https://ninjatek.com/wp-content/uploads/2016/05/NinjaFlex-TDS.pdf`, accessed 27/08/2017

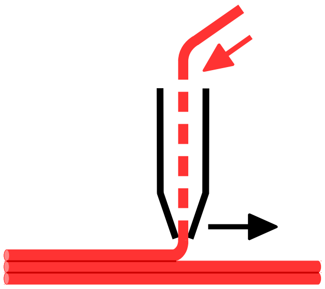

Figure 1.5: In FFF, the plastic filament (red) is fed through a small heated nozzle called the hot-end which is situated on the extruder head (black). The extruder moves in a specified pattern, leaving molten material in the required shape.

of these flexible materials is also more in line with biological materials mimicked by soft robots [7].

Indeed, as stated by Gorissen et al., additive manufacturing is already used to manufacture soft robots. Zolfagharian et al. differentiate between semi-3D-printed and 3D-printed soft actuators [25]. In semi-3D-printed actuators, the 3D-printing is considered a technology that helps the manufacturing, but still manual production steps (i.a. assembly) need to be performed by hand. In (fully) 3D-printed actuators, no post-processing is needed and there is thus only a single production step.

An example of semi-3D-printing of soft actuators is the printing of a mould to allow the casting of the actuator. She et al. fabricated a mould using FFF in which they cast Ecoflex-30 around a shape-memory alloy [26]. The advantage of moulding is that it is fairly easy to embed sensors and other electronics inside the actuator.

Another example, and also one of the first times that additive manufacturing was used to develop soft robotic parts, is the actuator of Stiltner et al. [27]. During the printing, the process is paused at just the right time for a person to manually put tendon cables inside the cable shafts foreseen. Afterwards, the printing is resumed to complete the actuator. This allows for a nice way to create living hinges, but also introduces the need to have a skilled operator closely watching the process.

In general, all types of additive manufacturing have the potential to be used to manufacture soft robots: i.a. polyjet printing ([28]), stereolithography ([29]), FFF ([30])... However, one of the main disadvantages of additive manufacturing is the limited choice in available materials. This is certainly the case in closed source systems, for which the materials can only be purchased through the machine manufacturer itself, but also for open source systems the choice is not too broad. This is considered in [31] as one of the main limitations, and certainly for soft robotics as the soft materials available for printing are even more limited. Nevertheless, Yap et al. have proven that it is possible to use these commercially available materials (in their case NinjaFlex) for the manufacturing of soft actuators [30].

Another problem as cited by Trimmer et al. is the multi-material printing. This is currently very limited and most often only consists of a main material and a soluble support material that supports the print during the fabrication process and is removed afterwards so that the actuator itself does not consist of multiple materials. One of the existing examples, is a jumping robot driven by combustion, which consists of a rigid and soft part printed together using FFF [32]. Another example is the octobot from Wehner et al. [33]. They use a more complicated manufacturing process for their robot by combining casting and printing of fugitive and catalytic inks.

The fast advance of 3D-printed soft robots, also creates a need for new (functional) materials that can be used in additive manufacturing. Several materials that have potential in soft robotics are already prepared for this use. Zarek et al. have prepared a soft shape-memory polymer that can be used in stereolithography by inducing a photopolymerization reaction [34]. At a temperature of 70 °C the printed parts can revert to their original shape, which is used in a practical set-up containing an electrical switch (conductive ink is printed on top of the polymer). This application shows great potential for use in soft robotics, but this is not the only application of these shape memory polymers. Yang et al. for example, have created a shape-memory polymer filament to be used in FFF [35]. Their use case is a soft compliant gripper.

Another interesting material that can be used in FFF is a SH gel, developed by Nadgorny et al. [36]. This gel is, although it can be classified under FFF, not extruded into a filament first. Instead, the gel is loaded into a syringe and extruded through the nozzle; it uses thus pressure rather than heat as an extrusion parameter.

1.4 Project goals

The main goal of this project is to develop a platform for the additive manufacturing of elastomeric SH DA materials using FFF, also commonly known under the term ‘3D-printing’. To achieve this goal, a first step is to investigate the important material properties.

Two sub-goals can be defined for this project. The first one being the extrusion of the filament that is used in the FFF process. The filament has to be of sufficient quality to print. The second sub-goal is the 3D-printing itself, in which the produced filament is used. The printing process should be able to print a proof of concept for a SH soft actuator.

After printing, the loss of SH capacity and change in material properties should be kept minimal. Therefore, it is also important to study the material properties after printing. These will be compared to those of unprocessed material.

The platform will be equipped with a dual extruder to be able to print two SH materials at the same time. These have the potential of healing one onto another. The focus will be upon studying the interface between the two materials when they are healed and on comparing it to other common techniques currently used in the field of soft robotics.

1.5 Outline

Due to the current limitations on the manufacturing of soft robotic actuators made out of the developed self-healing material, new research is conducted to open up more possibilities. Currently only shaping-through-folding-and-self-healing is applied, and this technique is rather limited in the complexity of the actuators that can be manufactured. One of the new manufacturing techniques which looks very promising, is the use of additive manufacturing.

To develop this technique, a first step is to take a look at the material properties. In Chapter 2, this is studied by looking at what is already known of the material and which properties are of interest for 3D-printing.

Once the properties are known, the material has to be extruded into a filament that can be used with the 3D-printer. For this process, several parameters have to be optimized, while also several problems occur; this is discussed in Chapter 3.

When the filament is prepared and considered consistent enough, it can be printed, this is described in Chapter 4. Before actually printing, a simulation is executed to get an idea of suitable process parameters. Afterwards, the real parameters are determined and test parts are printed to check the print quality. Next, material tests are performed to see whether the material properties have changed during the extrusion and printing process.

When the materials can be printed, preliminary research is conducted in Chapter 5 to go towards multi-material printing. More specifically, printing different self-healing materials at the same time. A first part of this research studies the interface between different self-healing materials.

Finally in Chapter 6, a reflection is made on how well the proof of concept has succeeded and what conclusions can be drawn from this project. In addition, the future work is considered, how it is expected to become even better and for what applications it can be used in the future.

Chapter 2

Materials and methods

In this chapter, the materials used for the 3D-printing process are described extensively. Before starting the actual printing process, it is important to study the working principle and characteristics of the Diels-Alder (DA) materials. This characterization is executed using various techniques, of which the theoretical background is given in this chapter.

2.1 Materials

2.1.1 Chemical structure

The elastomeric networks subject to this research consists of a network structure, containing two types of molecules. These molecules are heavily crosslinked with thermo-reversible covalent bonds created by the DA reaction. The reverse reaction is called the retro-DA reaction. The two reactions are in equilibrium with each other, and the equilibrium can be shifted by changing the temperature. The DA reaction is an organic reaction between a diene and a dienophile, as illustrated in Figure 2.1. The diene, with its two double bonds, is relatively electron rich, whereas the R_2 group on the dienophile makes it electron poor. This induces the cycloaddition reaction creating the DA adduct. The DA reaction is also stereoselective: there are two stereo-isomers of the DA adduct, called the endo- and exo-adduct.

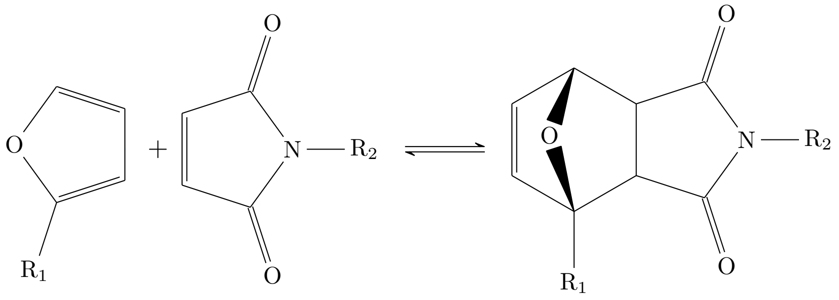

Figure 2.1: A DA reaction is an equilibrium reaction between a diene, which has two double bonds, spaced one carbon atom apart, and a dienophile, which has a double bond connected to an electron withdrawing group R_2. The electrons from the double bonds move cyclic and form a cyclohexene.

In order to heal, the material is heated to 80 °C. This shifts the equilibrium towards the reactants and increases the mobility, so the material can slowly fill the cracks. After 30 minutes at this temperature, the cracks are sealed, and the material can be slowly cooled down so the equilibrium shifts back towards the product, restoring the network. Because heat is required to perform the healing, the polymer is classified as a non-autonomous system, which is not necessarily a drawback as it allows for more control over the healing process.

As the material is a network polymer, it is amorphous and does not show a melting range. However, it does show a gelation point at the gel temperature (T_{gel}). If the material is cooled down below this temperature, it forms a single network molecule and the molecular weight shifts towards infinity (gelation). Above this temperature, enough bonds break so that there is no longer a single molecule network (degelation) and the mobility increases significantly. As kinetics are faster at higher temperatures, gelation happens the fastest at temperatures near (but still below) the T_{gel}. Degelation happens also faster at higher temperatures, but care has to be taken as there are irreversible side reactions (Michael addition, maleimide homopolimerization) that occur above 120 °C [37].

2.1.2 Synthesis

The synthesis of the self-healing (SH) DA material is based on three reactants (see Figure 2.2) and is performed in four steps, the detailed reactions are given in Appendix A.

1. A Jeffamine (Figure 2.2a) is combined with furfuryl glycidyl ether (FGE) (Figure 2.2b) to form a furan[1] functionalised compound, which acts as the diene in the DA reaction. The degree of polymerisation of the Jeffamine can be chosen, this impacts the spacer length, which eventually influences the crosslinking density and the mechanical properties of the material.
2. 1,1'-(methylenedi-1,4-phenylene)bismaleimide (DPBM) (Figure 2.2c), which acts as the dienophile, is dissolved in chloroform. This solution is mixed with the furan functionalized compound, and the DA reaction takes place partially.
3. Hydroquinone (Figure 2.2d) is added as a radical inhibitor to avoid irreversible reactions taking place.
4. The solution is cast into moulds, and placed in vacuum at 90 °C for 24 hours until all the chloroform is evaporated.

2.1.3 Mechanical properties

One of the interesting things about this material is the possibility to vary its mechanical properties. To do this is, it is enough to use a Jeffamine with a different degree of polymerisation. A longer Jeffamine increases the spacer length between the H_2N end-groups; when this length is short, the overall crosslink density, so the concentration of the thermoreversible covalent bonds is higher and the material will be stiffer and more brittle. A long spacer length gives a lower crosslink density and a more flexible material. Other properties that are changing with the spacer length are the glass transition temperature (T_g) and T_{gel}, both become lower with increasing

---

[1] Furan is a five-membered ring structure with one substituted oxygen atom and two double bonds.

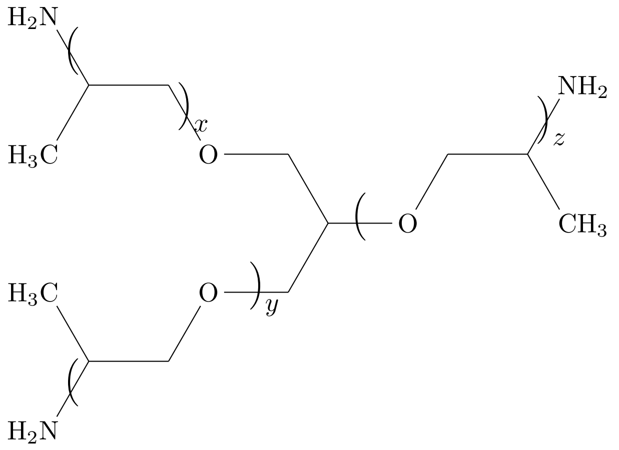
H$_2$N
NH$_2$
x
z
H$_3$C
O
O
CH$_3$
H$_3$C
O
y
H$_2$N

(a) Jeffamine T-series

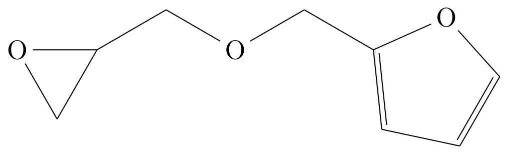

(b) Furfuryl Glycidyl Ether (FGE)

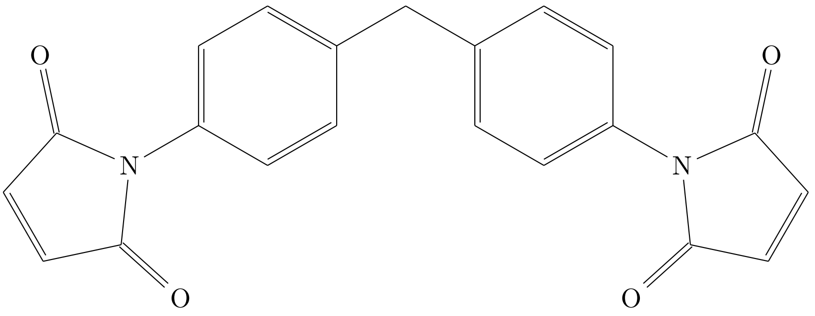

(c) 1,1'-(methylenedi-1,4-phenylene)bismaleimide (DPBM)

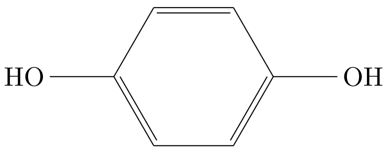

(d) hydroquinone

Figure 2.2: Three reactants and a radical inhibitor (hydroquinone) are used in the synthesis. The full synthesis reaction is shown in Appendix A.

spacer length [1].

It is also possible to use a T-series Jeffamine in the synthesis, these compounds have three H_2N end-groups instead of two (this is called the D-series). Due to this extra end-group, the resulting network has a higher (de-) gelation temperature when compared to a D-series. When comparing a D-series and T-series material of the same stiffness, the T-series will have a higher T_{gel}. This will come in handy for 3D-printing as the kinetics of the (de-)gelation will be faster at higher temperatures.

2.1.4 Recycling

Network polymers are cross-linked, and in most cases these cross-links are irreversible. This is a major drawback, as it makes recycling them impossible. However, in this DA material, the cross-links are thermoreversible, and thus the material can be recycled. To recycle it, the material is cut into small pieces, which are put in a flat mould. When raising the temperature above T_{gel}, the material flows and takes the form of the mould. After cooling, the DA material is recovered as a sheet, ready for use.

Terryn et al. proved that the change in mechanical properties after recycling is minimal. They found a drop in T_g of about 5 °C and in storage modulus of 19 % [1]. This is attributed to the forming of irreversible bonds in the material.

2.1.5 3D-printing

In Fused Filament Fabrication (FFF), the conventional materials are thermoplastics such as PLA and ABS. During 3D-printing, they are heated above their melting temperature (T_m) or T_g respectively for extrusion, and cooled down afterwards.

The described DA material is a network polymer and therefore does not melt, which means that the same principle can not be applied while 3D-printing this material. However, this material does have thermoreversible bonds that break upon heating because the equilibrium is shifted towards the reactants. This leads to degelation (at T_{gel}), and further lowers the molecular weight and thus the viscosity, which makes that the polymer can be extruded. After extrusion, the bonds will need to form again, which is realized by bringing the material below its T_{gel}, shifting the equilibrium back to the DA adduct.

It is clear that the physical process behind the 3D-printing process of the SH DA material is very different from the conventional materials, and this is a big challenge. As there is a chemical reaction taking place during the printing, this process can be classified as ‘reactive printing’.

2.2 Methods

2.2.1 Dynamic Mechanical Analysis

Theoretical background

Visco-elastic theory is used to characterize the material in a Dynamic Mechanical Analysis (DMA) and dynamic rheometry analysis. Therefore a small introduction is given to allow correct interpretation of the results. Visco-elasticity combines both the Newtonian fluid theory and Hooke’s law of elasticity, which are described by

$$\text{Newtonian fluid} \qquad \tau = \eta \cdot \dot{\gamma} \tag{2.1}$$

$$\text{Hookes law} \qquad \sigma = E \cdot \varepsilon \tag{2.2}$$

where

τ	Shear stress	σ	Tensile stress
η	Dynamic viscosity	E	Young's modulus
γ	Shear rate	ε	Strain

If a sinusoidal strain (with amplitude ε_A and angular frequency ω) is applied to a purely elastic solid material, Hooke's law dictates that the stress should be proportional (with amplitude σ_A) as the elastic modulus is constant.

$$E \cdot \varepsilon_A \sin(\omega t) = \sigma_A \cdot \sin(\omega t + \delta) \tag{2.3}$$

$$= \sigma_A \cdot \sin(\omega t + 0) \tag{2.4}$$

This implies that the phase angle δ between stress and strain is zero. For fluids on the other hand, Newtonian theory states that the shear stress (with amplitude τ_A) is proportional to the strain rate (with strain amplitude γ_A). Applying a sinusoidal stress gives

$$\eta \cdot \frac{\mathrm{d}}{\mathrm{d}t}(\gamma_A \sin(\omega t)) = \tau_A \cdot \sin(\omega t + \delta) \tag{2.5}$$

$$\eta \cdot \gamma_A \cos(\omega t) = \tau_A \cdot \sin(\omega t + \delta) \tag{2.6}$$

$$= \tau_A \cdot \sin(\omega t + \frac{\pi}{2}) \tag{2.7}$$

so $\delta = \frac{\pi}{2}$ for a purely Newtonian (viscous) fluid. Polymers nearly always have a characteristic that is visco-elastic, the degree of viscosity and elasticity is determined by looking at δ. The closer δ is to $\frac{\pi}{2}$, the more viscous it will behave, and the other way around, if δ is close to 0, the polymer will behave more like an elastic solid material.

For visco-elastic materials, the modulus is complex and can be written as follows

$$|E^*| = \frac{\sigma_A}{\varepsilon_A} \tag{2.8}$$

The real (E') and imaginary (E'') part of this modulus, given by

$$E' = |E^*| \cdot \cos(\delta) \tag{2.9}$$

$$E'' = |E^*| \cdot \sin(\delta) \tag{2.10}$$

are called the storage and loss modulus, respectively. The storage modulus E' is a measure for the (elastic) stiffness of the material, while the loss modulus E'' is linked to energy dissipated as molecular motion and heat. From Equations (2.9) and (2.10), it is deducted that

$$\tan(\delta) = \frac{E''}{E'} \tag{2.11}$$

Experimental conditions

DMA analysis is performed on a TA Instruments Q800 dynamic mechanical analyzer equipped with a film tension clamp. Two types of experiments are executed using this set-up. The first being a stress-strain test at room temperature, in which the strain is increased linearly with a rate of 60 %/min up until fracture of the sample, while the stress is measured. This allows to calculate the ultimate tensile strength, fracture strain, and Young's modulus.

The second experiment is a temperature ramp while applying a sinusoidal strain with a specified frequency and amplitude on the sample. During this analysis, the loss modulus, storage modulus, and tan(δ) are measured and plotted as a function of temperature. This allows for determination of the T_g, the temperature above which the polymer changes from a 'glassy' state to a 'rubbery' state. Different techniques exist for determination of the T_g, in this work, it is defined as the peak of the tan(δ) curve. The experimental procedure is to first equilibrate at -90 °C, followed by an isothermal period of 5 minutes. Next, the temperature is increased at a rate of 2.5 °C/min to 50 °C. The experiment ends with another isothermal period of 5 minutes. During all measurements, a frequency of 1 Hz and a strain amplitude of 0.2 % or 0.5 % are used.

2.2.2 Dynamic rheometry

This technique is complimentary to DMA, as both study essentially the same viscoelastic behaviour. DMA focusses more on the elastic range, whereas rheometry takes care of the viscous range of the visco-elastic behaviour. The temperature in a DMA test cannot be chosen too high as it becomes impossible to do a stress-strain analysis in tension on a material that flows.

Dynamic rheometry is used to determine the T_{gel}, this temperature is defined as the temperature where the phase shift δ is independent of the oscillation frequency [38]. For this experiment, a TA Instruments AR-G2 rheometer is used that measures G' and G'', the equivalents of E' and E'' in shear. Experiments are conducted on a circular sample with diameter 14 mm and consist of multiple frequency sweeps from 20 rad/s to 2 rad/s at constant temperature. After each frequency sweep, the temperature is increased by 2 K, starting from 80 °C and going up to 120 °C to measure gelation. To measure degelation, the measurements start at 120 °C, going down to 80 °C again in steps of 2 K.

2.2.3 Thermogravimetric analysis

In Thermogravimetric analysis (TGA), there are three important parameters: temperature, mass and time. During an analysis, the mass is measured constantly while the temperature is varied using a profile specified by the operator. The material sample for the analysis is in the range of a few milligrams and is prepared in a small container (pan) that is placed in the furnace while hanging from a balance arm. The analysis can be executed at a specified pressure and under a defined atmosphere which can be just air or inert gases such as nitrogen if desired. Using TGA, different physical properties can be studied, such as the thermal stability, absorption, and combustion. In this project, it is used to determine the thermal stability; at high temperatures, bonds begin to break and the material degrades. This is linked with a loss in mass as volatile components can leave the sample specimen.

The TGA analysis is performed using a TA Instruments Q5000 TGA, by equilibrating the sample at 50 °C before applying a temperature ramp of 10 °C/min to 600 °C. Afterwards, the sample is kept isothermal for 5 minutes at 600 °C before applying another temperature ramp of 100 °C/min down to 50 °C. The measurements are done under a nitrogen atmosphere.

2.2.4 Differential Scanning Calorimetry

Differential Scanning Calorimetry (DSC) compares the heat flow needed to change the temperature of a sample with that of a reference sample as a function of temperature. This allows to determine various transitions in the sample, such as the T_g, which is measured as a sigmoidal change of the base line. Also the exothermic reaction enthalpy of the formation of the DA bonds can be examined using this technique.

A TA Instruments Q2000 DSC is used to analyse the samples with the following procedure:

- Start at 25˚C, then perform a temperature ramp of 5 °C/min to 120 °C.
- Stay isothermal for 5 min.
- Temperature ramp of 5 °C/min to -90 °C.
- Stay isothermal for 5 min.
- Temperature ramp of 5 °C/min to 120 °C.
- Stay isothermal for 5 min.
- Perform a temperature jump to 25 °C.

2.2.5 Kinetic simulations

To simulate the kinetics, a software was developed in-house by ir. Robrecht Verhelle. This software is used to simulate the kinetics of (complex) chemical reaction processes. In the current work, the kinetics of the DA reactions were simulated for different temperature histories, as well as for filament extrusion and 3D-printing. The software considers a mechanistic model consisting of the following equilibrium reaction between Furan (F), Maleimide (M) and both stereo-isomers of the DA-adduct (A_{endo} and A_{exo}) [39].

$$A_{\text{endo}} \xrightleftharpoons[\text{k}_{\text{DA, endo}}]{\text{k}_{\text{reverse DA, endo}}} F + M \xrightleftharpoons[\text{k}_{\text{reverse DA, exo}}]{\text{k}_{\text{DA, exo}}} A_{\text{exo}} \tag{2.12}$$

Where each k indicates a reaction rate constant. The model uses the following differential equations to calculate the concentrations of the different components.

$$\frac{\mathrm{d}\left[C_i\right]}{\mathrm{d}t} = \sum_{i=1}^{N} v_i \tag{2.13}$$

with

$\frac{\mathrm{d}\left[C_i\right]}{\mathrm{d}t}$	Production rate of component i	$\left[\frac{\text{mol}}{\text{kg} \cdot \text{s}}\right]$
$[C_i]$	Concentration of component i	$\left[\frac{\text{mol}}{\text{kg}}\right]$
N	Number of reactions	
v_i	Reaction rate of reaction i	$\left[\frac{\text{mol}}{\text{kg} \cdot \text{s}}\right]$

The reaction rates v_i are defined as the reaction rate constant k (as shown in Equation 2.12) times the concentrations of the reactants of reaction i.

These reaction rate constants (k_i) are dependent on the temperature (T) based on the Arrhenius equation

$$k_i(T) = A_i \cdot e^{\frac{-E_i}{RT}} \tag{2.14}$$

where E_i is the activation energy, A_i a pre-exponential factor, and R the gas constant. The parameters used in the simulations are given in Table 2.1.

Moreover, the simulation program calculates the degree of conversion x for both adducts and the total conversion x_{tot} as

$$x_{\text{endo}} = \frac{[A_{\text{endo}}]}{\min\left([F]_0, [M]_0\right)} \tag{2.15}$$

$$x_{\text{exo}} = \frac{[A_{\text{exo}}]}{\min\left([F]_0, [M]_0\right)} \tag{2.16}$$

$$x_{\text{tot}} = \frac{[A_{\text{endo}}] + [A_{\text{exo}}]}{\min\left([F]_0, [M]_0\right)} \tag{2.17}$$

These conversion degrees are used in a simulation in Section 3.2, and are also a way to see whether the material is gelled or not. The degree of conversion at gelation is defined as

$$x_{\text{gel}} = \frac{1}{\sqrt{(f_F - 1)(f_M - 1)}} \tag{2.18}$$

where

f_F	Functional groups of furan
f_M	Functional groups of maleimide

f_M is equal to two in all materials used during this research, while f_F is four for a D-series Jeffamine and six for a T-series Jeffamine. This makes that $x_{\text{gel}} = 0.577$ for a D-series and $x_{\text{gel}} = 0.447$ for a T-series Jeffamine.

The simulation program takes as input the time-based temperature profile $T(t)$ and assumes a fully uncured (0 % conversion of both DA adducts) mixture at the start of the simulation. To have a simulation of the printing that starts with a cured state of the material, every simulation is preceded with the material being at room temperature for 24 hours. This makes sure that the material is near equilibrium at the beginning of the actual simulation and moreover, that every time the starting conditions are identical.

Table 2.1: The simulation program uses these parameters to calculate the process kinetics. The pre-exponential factor A is calculated for each reaction using Equation 2.14 by a known value for k at 298.15 K, which are given in this table.

Parameter	Value	Unit
Activation energy $E_{\text{DA, endo}}$	59600	$\frac{\text{J}}{\text{mol}}$
$\log_{10}(k_{\text{DA, endo}})$ at 298.15 K	-4.1748	$\log_{10}(\frac{\text{kg}}{\text{s mol}})$
Activation energy $E_{\text{reverse DA, endo}}$	109000	$\frac{\text{J}}{\text{mol}}$
$\log_{10}(k_{\text{reverse DA, endo}})$ at 298.15 K	-4.1784	$\log_{10}(\frac{1}{\text{s}})$
Activation energy $E_{\text{DA, exo}}$	56200	$\frac{\text{J}}{\text{mol}}$
$\log_{10}(k_{\text{DA, exo}})$ at 298.15 K	-4.7184	$\log_{10}(\frac{\text{kg}}{\text{s mol}})$
Activation energy $E_{\text{reverse DA, exo}}$	125000	$\frac{\text{J}}{\text{mol}}$
$\log_{10}(k_{\text{reverse DA, exo}})$ at 298.15 K	-7.5354	$\log_{10}(\frac{1}{\text{s}})$

2.3 Characterisation

The main material that will be used in this research is DPBM-FGE-JT5000. This material will be extruded into filament and printed, therefore it is important to characterize it to know the properties during the printing processes.

2.3.1 Thermogravimetric analysis

A TGA analysis on a sample of the SH material DPBM-FGE-JT5000 is given in Figure 2.3. A small weight loss already happens at low temperature. At 189 °C, 1.4 % of the weight is already lost. This is the result of the last solvent chloroform present in the sample escaping[2]. At temperatures higher than 200 °C, the material starts to degrade. Thus it can be concluded from this analysis that for further research and use of the material, higher temperatures should not be considered.

2.3.2 Dynamic Mechanical Analysis

The T_g can be determined using the DMA results from Figure 2.5. The T_g is defined as the point where $\tan(\delta)$ is maximal, so T_g is found to be -47 °C. This is well below every expected use case temperature. At room temperature (25 °C), the material has a storage modulus of 20.4 MPa, loss modulus of 2.8 MPa and a $\tan(\delta)$ of 0.14.

---

[2] The escaping of chloroform does not pose a health hazard at lab scale. However, if this material would be produced at industrial scale, a harmless solvent would need to be used.

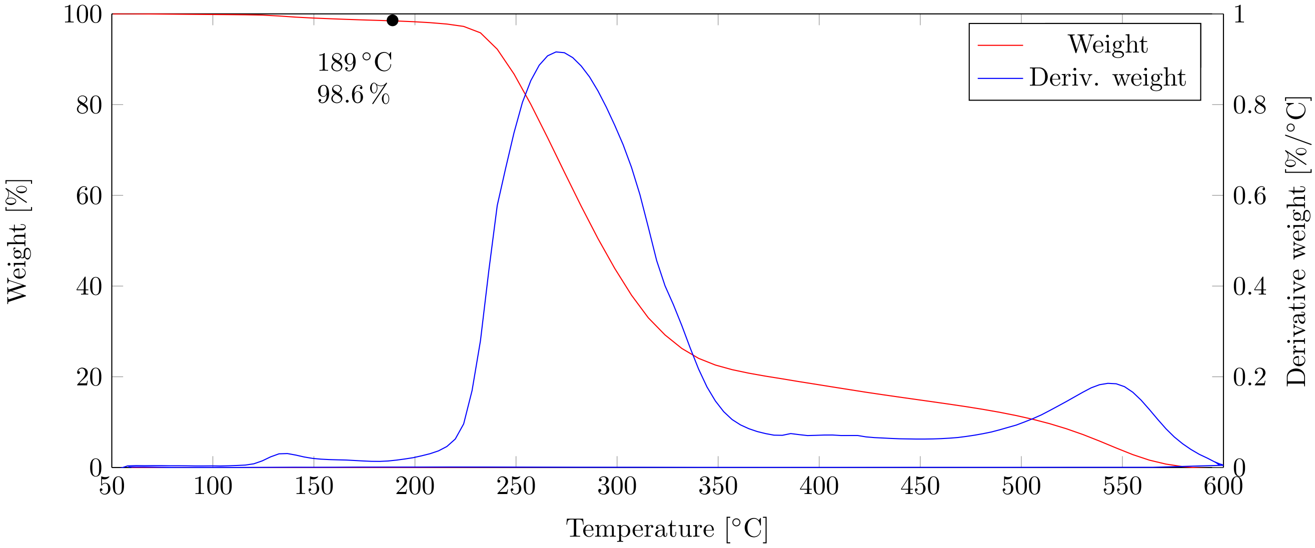

Figure 2.3: TGA analysis of JT5000. These TGA results are obtained using the following procedure: 1. Equilibrate at 50 °C; 2. Ramp 10 °C/min to 600 °C; 3. Isothermal for 5 min; 4. Ramp 100 °C/min to 50 °C.

Via a static stress-strain test until fracture, the Young's modulus is determined as 7.9±0.4 MPa (at room temperature). The ultimate tensile strength is 2.0±0.2 MPa at a fracture strain of 144±10 %.

2.3.3 Rheometry

Using this technique it is possible to determine the T_{gel}. This temperature is defined as the temperature at which the phase shift δ is independent of the oscillation frequency [38]. In degelation, this temperature is determined to be 104 °C and in gelation 105 °C, which is shown in Figure 2.6. From this analysis, it can be concluded that the material should be printed and extruded above this T_{gel} as there the viscosity will decrease significantly and the material can flow.

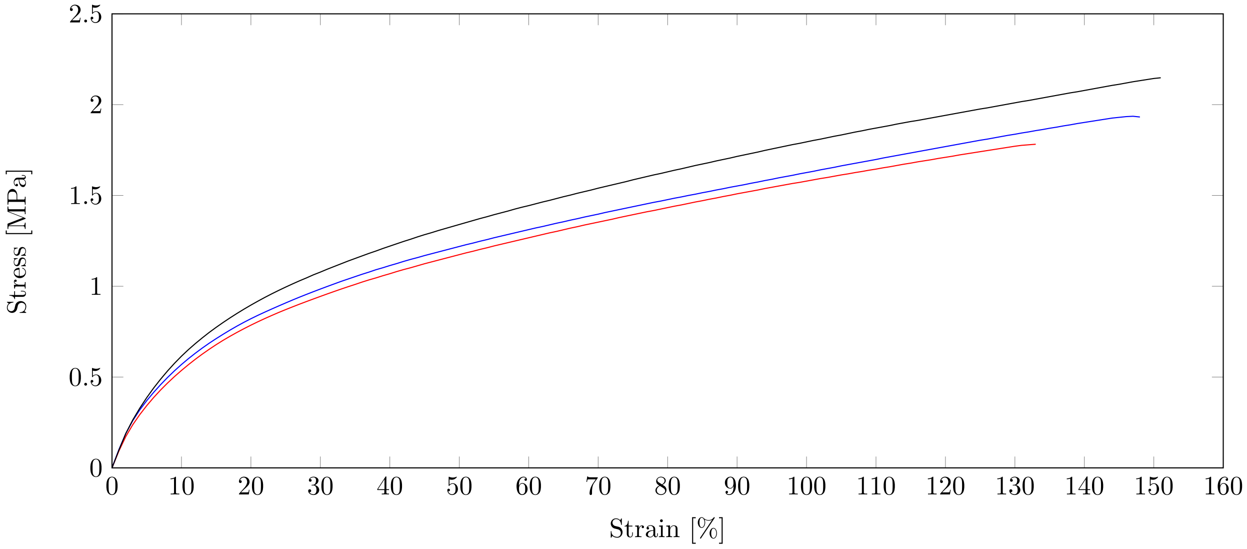

Figure 2.4: Stress-strain curves of samples JT5000. Three samples were tested at a strain rate of 60 %/min at an ambient temperature of 25 °C . The ultimate tensile strength is 2.0±0.2 MPa at a strain of 144±10 %. The Young's modulus is 7.9±0.4 MPa.

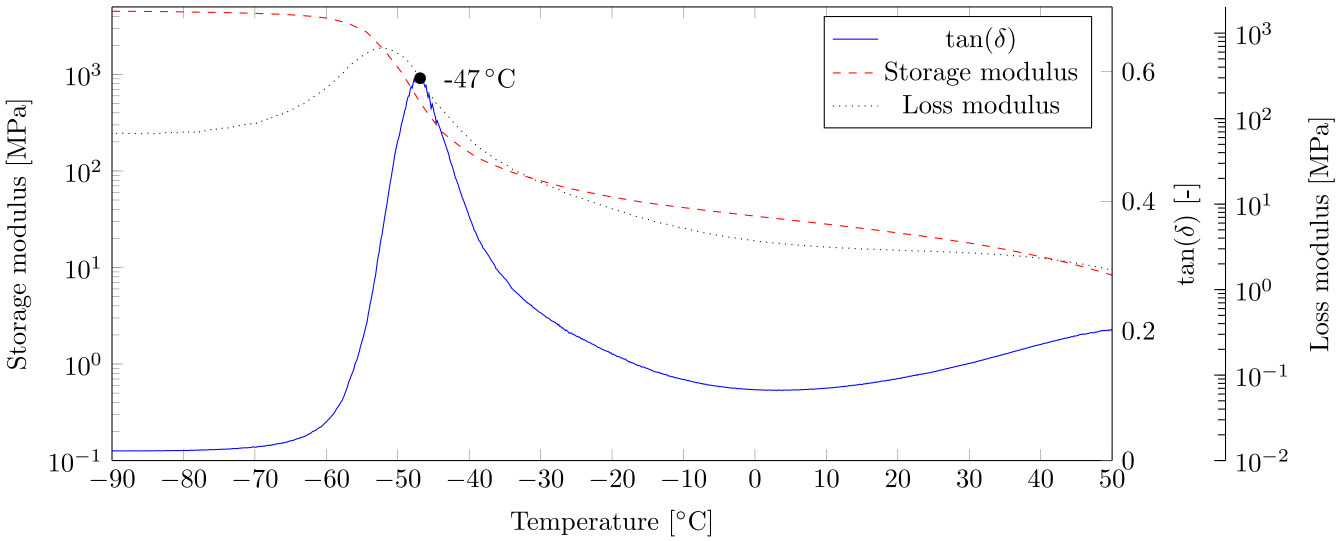

Figure 2.5: The DMA analysis of JT5000 shows a T_g of -47 °C. Measurement performed on a sample of size 8.94×5.55×0.55 mm with an oscillatory strain of 0.2 %, frequency of 1 Hz, static force of 0.01 N, 125 % force tracking, and a temperature ramp of 2.50 °C/min.

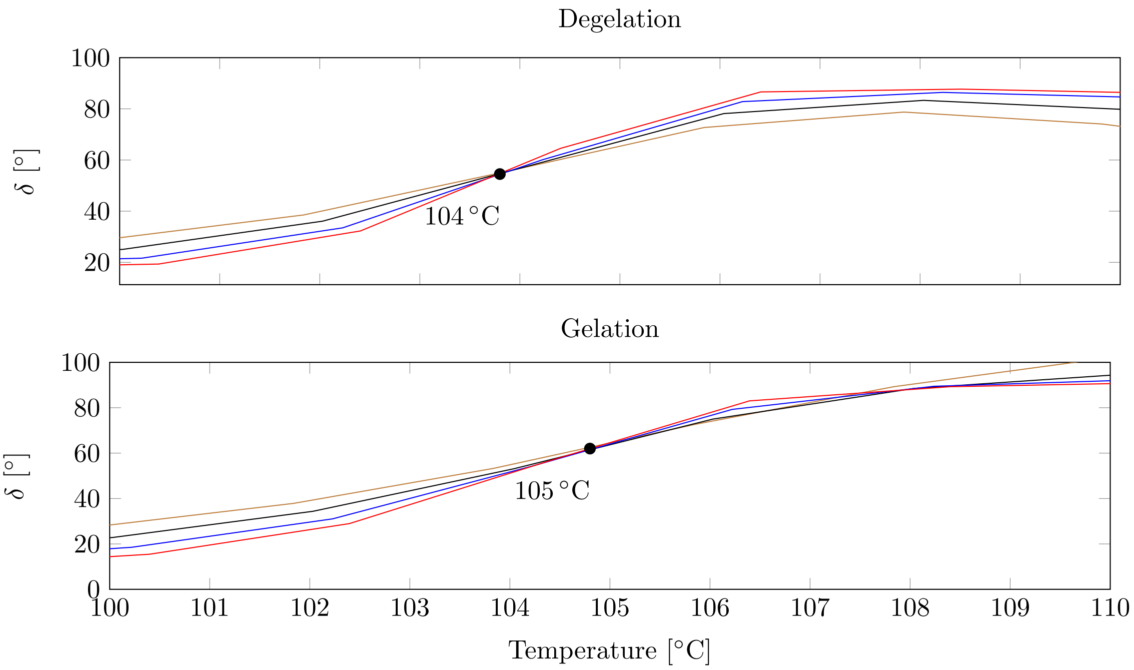

Figure 2.6: The rheometric analysis of JT5000 was performed at various angular velocities ranging from 1.99 rad/s to 19.87 rad/s, depicted as different colours. T_{gel} is determined as 104 °C in degelation and 105 °C in gelation.

2.4 Conclusion

From the characterisation of the material, it is concluded that it is indeed a good candidate for this research and application. With its Young's modulus of 6.4 MPa at room temperature, it is ideal for soft robotics, and the relatively high T_{gel} allows for fast kinetics, which can speed up the process. The ideal temperatures for the filament extrusion and printing process should be above the T_{gel} of 105 °C, but below 120 °C to avoid irreversible reactions.

Chapter 3

Filament extrusion

Now that the characterization of the material is done, the filament needed to feed the 3D-printer, can be extruded. The development of the extrusion process and improvements are described in this chapter. For this, a Noztek Touch filament extruder (see Figure 3.1) is used, which is available at the lab. The extruder consists of two heaters, whose temperatures can be set independently, and a motor with adjustable rpm. The machine also comes with two interchangeable dies that can be screwed into the machine. This is to have options in diameter size (1.75 mm and 2.85 mm). 2.85 mm was chosen as this is the diameter needed for the printer selected in Section 4.1.

For conventional polymers used in additive manufacturing, such as ABS and PLA, the material is fed to the filament extruder as grains. In order to mimic this, the solvent-cast sheet of self-healing (SH) polymer JT5000 is cut into squares of about 1 mm × 1 mm. These cubes are then fed into the extruder, which uses a single screw to feed the cubes evenly to the heater. The new cubes fed into the heater push the heated material at the front out, through the die. The extruder has three settings: heater temperature, pre-heater temperature, and motor rpm. Moreover, the machine also has a fan that can be switched on to cool down the extruded filament.

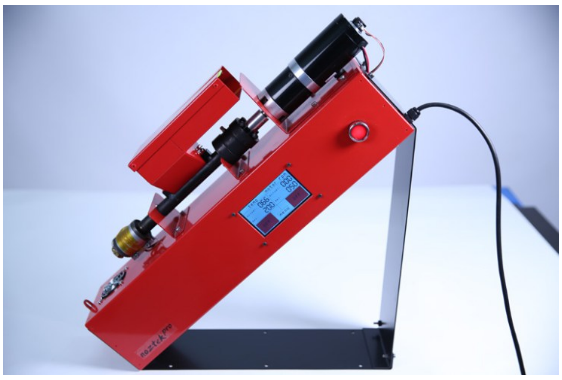

Figure 3.1: The Noztek Touch is a single screw extruder used to produce the filament. It is equipped with two heaters, a fan, and an extrusion motor.

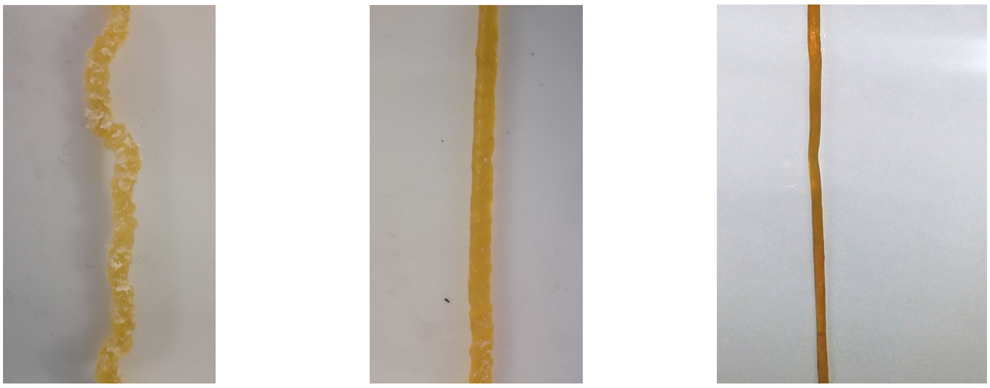
(a) (b) (c)

Figure 3.2: The filament extrusion parameters are important to get right. Different examples of failure phenomena are shown. (a) Too low temperature. (b) Sharkskin. (c) Diameter variation.

3.1 Initial tests

First, initial tests were executed with the extruder to see how the material reacts to extrusion. During these first tests, the extrusion temperatures were set below the gel temperature (T_{gel}), to 95 °C. Then, the temperature is slowly raised step by step to get an idea at which temperatures the material is extruded best.

Slightly below the T_{gel} of 105 °C, the kinetics are fast but the material is still a macroscopic network. If the material is not enough heated, the viscosity is too high for the extrusion and the shear failure phenomenon (a) in Figure 3.2 is observed. Here, the material never fully degelled and the cubes are just deformed inside the screw and healed onto each other inside the heater, which is why the original form of the cubes is still very prominent.

In Figure 3.2b, the temperature was raised to above the T_{gel}, and it can be seen that the cubes become less prominent, but the filament is not yet very smooth; the sharkskin phenomenon is observed (Section 3.3.3). Moreover, the filament is also twisting, which can be an expression of a stress relaxation phenomenon, which is a typical visco-elastic property (Section 3.3.1).

If the temperature is raised even more with a few degrees, the filament as shown in Figure 3.2c is obtained. It is now seen that the filament is more smooth, but the diameter is inconsistent. Sometimes, variations of up to a millimetre can happen in the range of 10 cm of filament. This consistency is one of the key parameters that characterize filament quality. As a 3D-printer does assume that the specified diameter is exact, it will always extrude the same length for the same volume of material that needs to be extruded. However, if the diameter varies, some parts of the print will have too much extruded material whereas other parts may not have enough, leaving a low quality print. In the worst case, a filament that is too thick can block the extruder.

Eventually, a first batch of filament was prepared using the following settings

Pre-heater	110 °C	**Motor speed**	10 rpm
Heater	107 °C	**Fan**	off

This was achieved after heating the diced material up to 120°C and leaving it to cool at room temperature for about 4 hours after doing a previous filament extrusion test. Due to the rather slow kinetics of the reaction, the material is not yet in equilibrium at this point, which proved very promising as this batch had the best results up to that moment. It was decided to investigate what happened inside the material and to propose a pre-heating procedure mimicking this that should be executed prior to extrusion.

3.2 Simulation of the pre-heating procedure

To find an optimal pre-heating procedure, the degrees of conversion of both Diels-Alder (DA) adducts are simulated using a software script developed at the FYSC department and described in Section 2.2.5.

In this case, the temperature profile is specified to 120 °C for 20 minutes and then put at room temperature to cool down for another 4 hours. Here, the conversion degrees of the DA adducts are of interest, as the material will be gelled but not yet in equilibrium. After doing the simulation, which is shown in Figure 3.3, it can be seen that the conversion degrees of endo- and exo-adduct are both 0.30, this gives a total conversion of 0.60, which is above x_{gel} as defined in Section 2.2.5, so the material is gelled at this point. In theory, this process of heating to 120 °C and cooling down could be used, but it is quite time consuming and is not ideal for larger batches. The reason is that after this heating procedure, the material has completely lost its shape because of the degelation at 120 °C (this is above T_{gel}). This means the cubes have to be cut during (the end of) this 4 hour waiting period. Instead, it is preferred to have a heating procedure that is faster, at lower temperatures to avoid irreversible reactions, and that results in similar conversions at the end.

The process of finding an optimal heating procedure is made easier as it can be seen that (per coincidence) the conversions of both DA adducts are equal at the end of the procedure. When keeping the material at a constant elevated temperature in the simulation, it can be noticed that for each constant temperature, there is a single point where it happens that both adduct conversions are equal.[1] It is also noticed that the higher the temperature, the less time is needed to reach this point, but also the lower the degree of conversion at which this crossover happens.

These points of equal conversion are given in Table 3.1. It can be seen that leaving the material at 80 °C for about 35 minutes creates similar conversion degrees as the original procedure. This will be selected as the pre-heating procedure, and the material is extruded immediately after this pre-heating step. After testing, it is verified that this procedure gives indeed a filament with the same properties as with the original procedure.

---

[1] This point is present in Figure 3.3, but rather difficult to see as it happens almost instantly after heating due to the high temperatures.

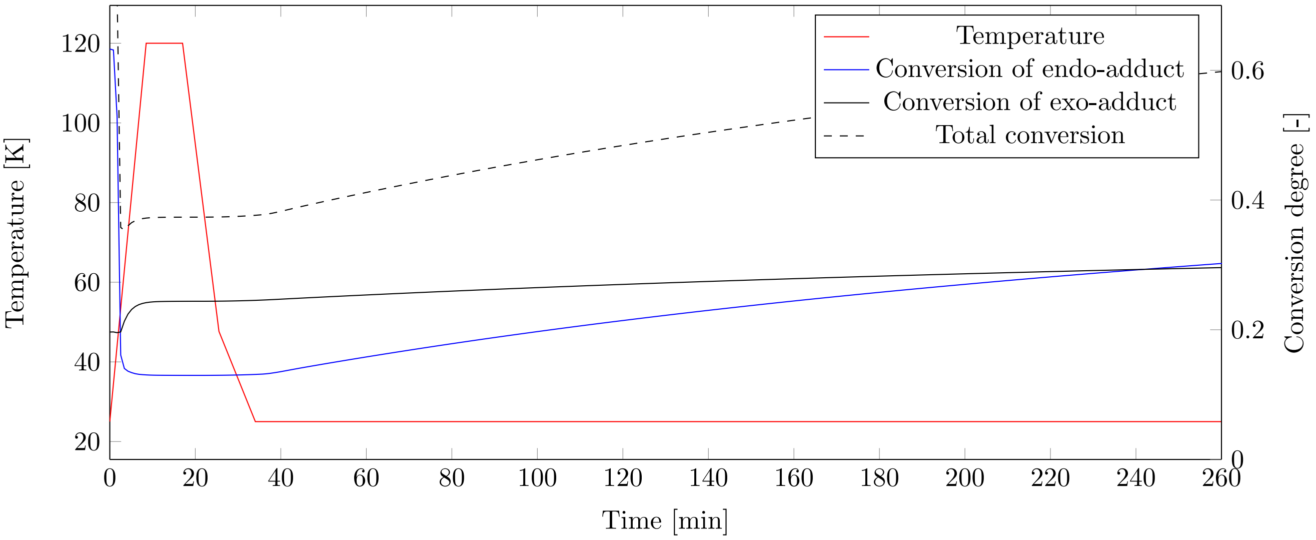

Figure 3.3: The kinetics of JT5000 are simulated: after 24 hours at room temperature (not shown), the conversion of endo-adduct is 0.63 and for exo-adduct, the conversion is 0.20. Then the temperature is raised to 120 °C for 20 minutes and cooled down again to room temperature where it is left to rest for another 4 hours. At this moment, the conversion of both endo- and exo-adduct is 0.30.

Table 3.1: Equal conversion points at various temperatures.

Temperature [°C]	Conversion [-]	Time [min]
70	0.34	102
75	0.32	59
80	0.30	34
90	0.27	12

3.3 Failure phenomena

During the initial testing, but also after establishing the pre-heating process, different failure phenomena were observed. To improve the filament extrusion process as much as possible, these different phenomena are identified and studied so they can be counteracted if possible. Based on the outcome of this study, several solutions can be selected and implemented, which are described in Section 3.4.

3.3.1 Stress relaxation

A first phenomenon that is observed during extrusion, is stress relaxation, this is a typical property for visco-elastic polymers and means that there is a delay between strain and applied stress. This poses a problem in the filament extrusion process, which is clearly visible in Figure 3.2a. As the cubes are fed to the heater via a rotating screw, they will afterwards still curl up in the heater and also after extruding due to elastic memory effects in the viscoelastic material. This means that the filament will be curled, which is undesired. To overcome this, the memory of this twist needs to be lost. A higher temperature or longer contact with the die are possible solutions.

3.3.2 Die swell

Die swell or the Barus-effect is also a visco-elastic property. It is affected by the shape of the orifice, which is a circle in this case, and thus posing less of a problem as deformation is only expressed in an increase in diameter of the filament after extrusion. Therefore, this phenomenon can be expressed in the ratio

$$\frac{D_{\text{extruded}} - D_{\text{die}}}{D_{\text{die}}}$$

Moreover, die swell does also depend on the die design and cooling rate. The die should have a land (parallel section) which is as long as possible, so that the material does not deform afterwards, which makes it actually also a stress-relaxation problem. The cooling rate can be problematic as the outer material cools down faster than the inner material, this may createbubbles and a blown up effect [40].

For the SH polymer, the die swell ratio was determined to be approximately 0.14, so with a die diameter of 2.5 mm to counteract this effect, the diameter of the resulting filament should be 2.85 mm. Although the Barus effect is strongly temperature and flow rate dependent, this should already give a better dimension for the filament compared to the 2.85 mm die.

Other solutions can be reducing the extrusion speed and as already stated, having a longer die land. These lead to a longer contact with the die, giving similar solutions as for the stress relaxation. Alternatively, increasing the extrusion temperature may also help as it lowers the viscosity of the polymer.

3.3.3 Sharkskin

The sharkskin effect is a melt flow instability and is described by Koopmans and Molenaar as "a surface with a more or less regular pattern of ridges resulting in an observable mattness or roughness" [41]. It is typically observed at higher flow rates and starts at the die outlet [42]. It is generally believed that adhesion of the material to the die outlet wall is the cause. The material forms a ring, growing when more material passes. When this ring is big enough, it detaches from the wall, leading to the specific pattern linked to sharkskin [43].

The phenomenon has been studied in-depth for different (semi-crystalline) polymers [41][43]. These studies have shown that sharkskin poses a bigger problem the more the polymer molecules are entangled. Moreover, it was shown that at low flow rates, the shark skin phenomenon is absent, and that the extrusion pressure acting on the material is linearly increasing with this flow rate. At a certain moment while increasing the flow rate, there is a pressure plateau where the pressure remains constant for a certain flow rate range. At this moment suddenly sharkskin starts to form. At even higher flow rates, the sharkskin disappears but other failure phenomena will start to take place.

Proposed solutions to this problem are lowering the flow rate, but also applying a PTFE coating at the die exit to lower the friction [44]. Another solution proposed by Agassant et al. is to add fluoropolymer additives to the material. This solution is however not feasible for this case as this new material would have to be developed and characterized.

3.4 Solutions

Due to the different described failure phenomena, the filament is not good enough to be considered for printing. To overcome these problems and extrude a usable filament, different solutions are implemented.

3.4.1 Extrusion speed

Lowering the extrusion speed is a logical choice as it can improve all three explained failure phenomena. However, the Noztek machine has a lower limit on the extrusion velocity (measured as the rotational velocity of the screw) of 10 rpm. This proved to be too fast to prevent the different described failure phenomena. This lower limit is set by Noztek in the software of the extruder, but without having access to the source code, altering this limit is impossible without reverse-engineering the whole machine and rewriting the controller.

To overcome this, it was decided to disconnect the motor driving the screw and the rotary encoder reading the rotational velocity from the machine. Instead, an H-bridge is used to drive the motor. This H-bridge is connected to an Arduino UNO, as well as the rotary encoder and a potentiometer. The H-bridge is fed using the original 24 V power source of the machine and the Arduino using an external USB cable. The motor is controlled using a simple PID controller and the potentiometer is used to be able to set and alter the speed easily. This way, very low rotational speeds can be achieved, which was not possible with the original software, a more detailed overview is given in Appendix B.

3.4.2 Die design

By having studied the different failure phenomena that were observed, it has become clear that the die design is a very important factor in the extrusion process. The two original dies that were shipped with the Noztek extruder are shown on the left in Figure 3.4. These were extensively used for the initial testing.

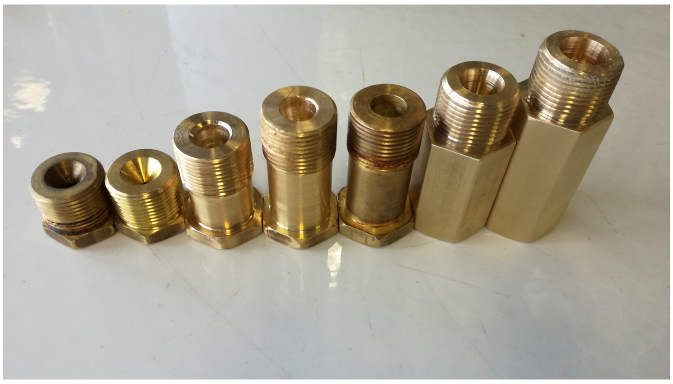

Figure 3.4: Evolution in the die design from left to right. The newer dies have an increased land length and smaller angle of entrance.

A first improvement is to increase the land length and add a buffer zone so that the material has a longer contact with the die for the same extrusion velocity. This increases the time for stress relaxation, and is beneficial for the reduction of both the sharkskin and die swell phenomena. The drawback is that more pressure is needed to push the material through as there is more friction, but this did not pose any problems. Something that did pose a problem, is the temperature. When having a longer die, the heater is further away from the exit and thus there is a bigger temperature gradient over the die. In the longest die in Figure 3.4, the problem was that the exit was too cold so that the material was gelling and blocking the extrusion. Insulating foam is put around the die to solve this problem.

Another adaptation to the die is to add a smaller relief angle. This is the angle of the die at the exit relative to the extrusion direction, and is 90° in the original dies. A smaller angle allows to guide the material more after exiting the die. Also the entrance angle is changed to have a more gradual intake, this reduces the shear force on the polymer and the dead zone (where the material is not flowing). Lowering this angle also increases the length of the die significantly without having a longer land.

As already stated, the die diameter is reduced to counteract the die swell. With a diameter of 2.5 mm it is expected to get a final diameter of 2.85 mm for the filament, although this may vary based on other extrusion parameters.

3.4.3 Drawdown

Drawdown is the stretching of the extruded polymer to reduce the size (in this case just the diameter). This can be applied to counteract the die swell. The force needed to stretch the polymer depends on the molecular entanglement and molecular weight, it is thus lower at higher temperatures for the SH material.

As extruding the filament orders the molecules along the longitudinal axis, it also increases the strength in this direction, while the transversal strength is decreased. This is not expected to have a big influence.

This stretching can be applied advantageously. As it depends on the force pulling on the

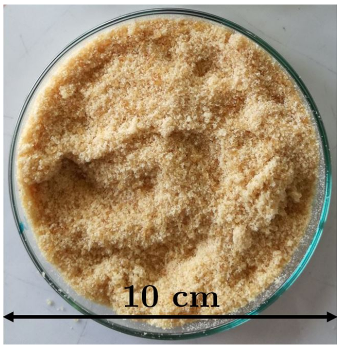

Figure 3.5: The DA material is brought to below its T_g by using liquid nitrogen and then grinded to produce fine particles.

extruded filament, the distance from the die exit to the resting position is important. Having a longer distance means that there is more force pulling because of the gravity acting on the extruded filament. So by changing the height of the extruder, the drawdown can be more or less controlled.

3.4.4 Grinding

The smaller the size of the cubes that are fed in the extruder, the more uniform the material is heated and the more uniform the pressure in the extruder screw will be. Cutting the cubes by hand is a tedious and labour intensive task, and moreover the minimal cube size is limited. Therefore, it is a good idea to grind the material instead. As grinding the soft material at room temperature did not work, it is first cooled down below its glass transition temperature (T_g) using liquid nitrogen and afterwards grinded. This produces fine particles that can be fed in the extruder (see Figure 3.5).

The question arises whether this grinding operation breaks only the reversible bonds, or if also other bonds are broken. If the latter is the case, there will be an impact on the material properties. So before applying the grinding technique further on in the extrusion process, this has to be validated. For the validation, a batch of material is split in two parts. One part is grinded while the other part is cut into pieces of $1\,\mathrm{cm} \times 1\,\mathrm{cm}$ and acts as the reference. Both parts are then put into different moulds and heated up to 110 °C for 60 minutes to form again sheets. The sheets are stored at 30 °C.

Differential Scanning Calorimetry (DSC) analysis is performed on both the grinded material and the reference following the procedure described in Section 2.2.4. Figure 3.6 shows that the heat flow for both samples is nearly equal. Also a Dynamic Mechanical Analysis (DMA) analysis is performed to cross-check the findings and have a better view on a possible change in material properties, this is depicted in Figure 3.7. Again, the change in material properties is negligible and it can thus be concluded that grinding the material has no influence on the material characteristics. This result is also useful for future research that will be performed by research group SMaRT from KULeuven and focusses on Selective Laser Sintering (SLS), as this technique requires the material to be a powder.

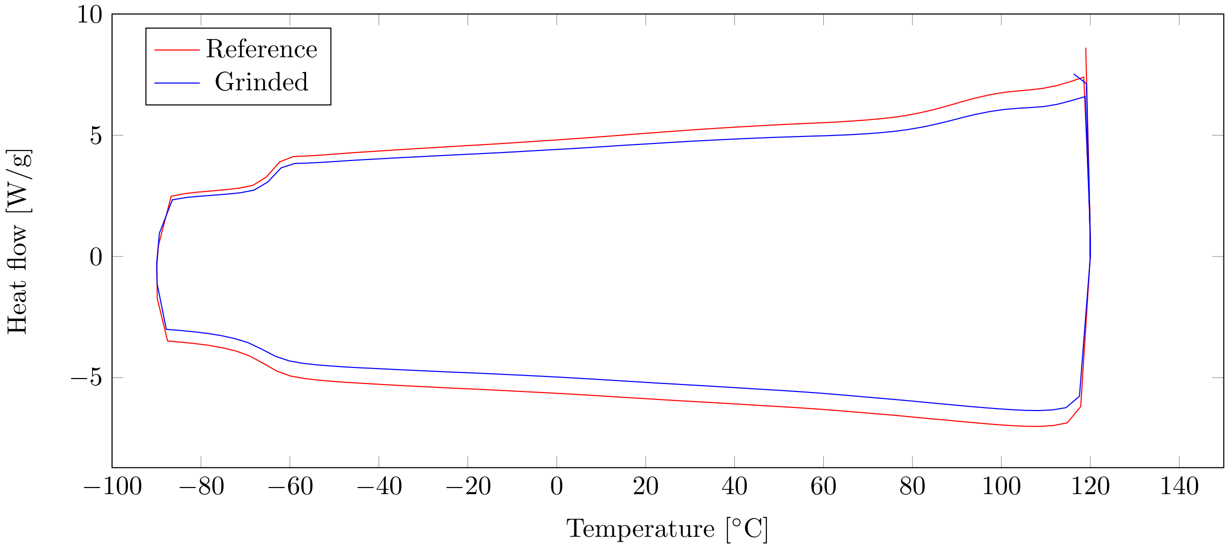

Figure 3.6: DSC analysis of a sample grinded material compared with a reference shows that the grinding operation does not have any influence. Sample mass: 21.09 mg for the grinded sample and 22.45 mg for the reference sample.

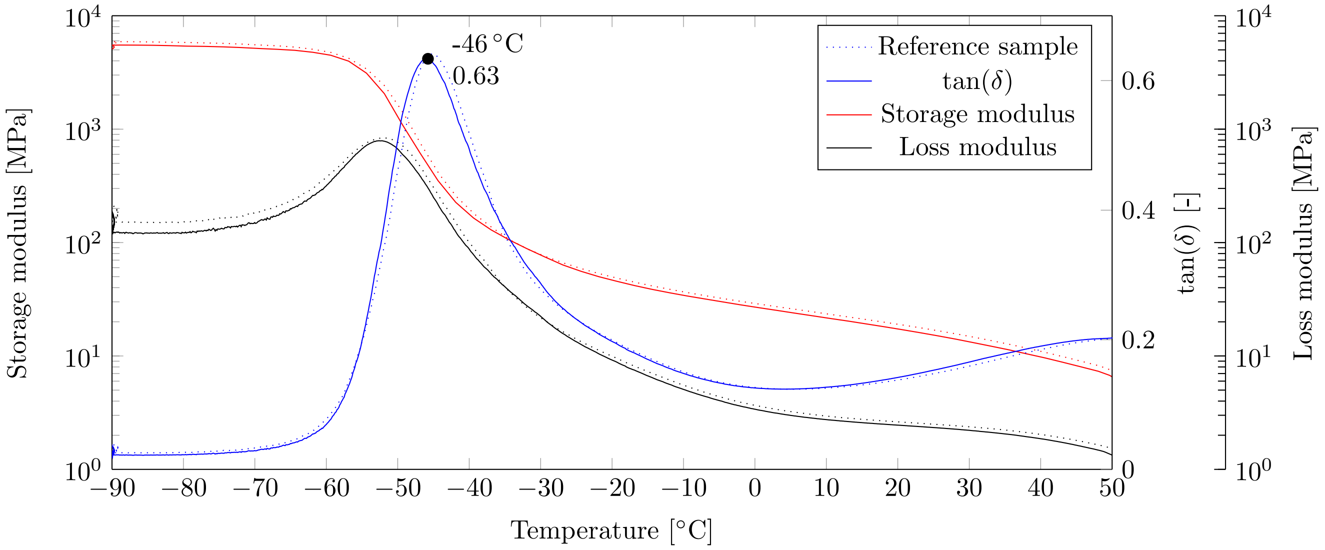

Figure 3.7: DMA analysis of a grinded sample JT5000 (10.6 mm×5.9 mm×1.2 mm) compared with a reference sample (9.4 mm×6.1 mm×1.2 mm) shows a T_g of −46 °C. Measurement performed with an oscillatory strain of 0.5 %, static force of 0.01 N, 125 % force tracking, and a temperature ramp of 2.50 °C/min.

3.5 Recycling

Because the DA material is rather expensive to produce, it is preferred to have minimal losses. All failed filament is not discarded, but can be easily recycled. This four-step process is illustrated in Figure 3.8 The material is re-heated in a mould above the T_{gel} so that it can form a sheet. This sheet is afterwards cut again in small cubes or grinded into a powder that is fed in the extruder.

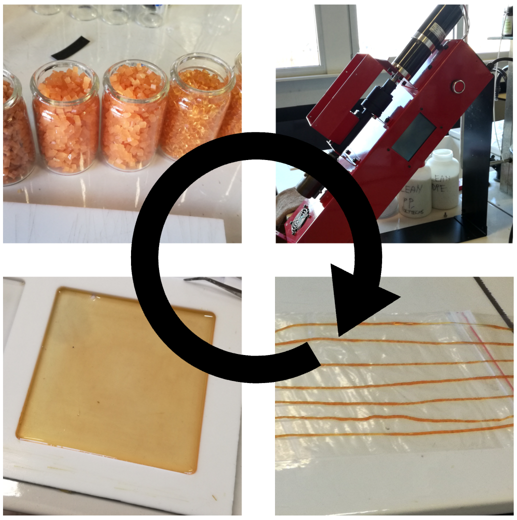

Figure 3.8: Bad filament or failed prints can easily be recycled in a four-step cycle. 1. Re-mould the material in a sheet by heating it up above the T_{gel}. 2. Cut the sheet in small cubes. 3. Feed the cubes in the extruder machine. 4. Extrude new filament.

3.6 Results of the filament extrusion

Filament extrusion should be a continuous process in order to limit the start-up and end-of-production effects. At the end of the batch, there is no more material pushing the material through so the extrusion becomes slower and filament will have different properties as the temperature profile it underwent is different. The batches made were always a few metres long, and rolled on a spool after extrusion, as shown in Figure 3.9.

As described in this chapter, several problems occurred during the extrusion process that lead to diameter variation. Different solutions are implemented to overcome these problems and this allows to extrude filament that is good enough to be printed.

The final settings for the filament extrusion of JT5000 are

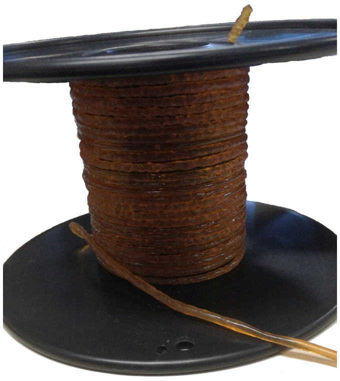

Figure 3.9: A batch of filament produced during the filament optimization process. Sharkskin is still present but the general diameter variations in the bulk of the material are good.

Pre-heater	118 °C	**Motor speed**	1 rpm
Heater	109 °C	**Fan**	off

Also, improving the filament is still work in progress. The filament produced during this project is reasonably good, and is good enough to be printed. However, the diameter variation is still a problem although a lot of improvements and iterations were implemented. One solution for this would be to replace the Noztek machine with another one that has diameter feedback and control, such as the 3DEVO NEXT filament extruder[2].

---

[2] `https://3devo.com/next-filament-extruder/`

Chapter 4

3D-printing of self-healing polymers

To obtain a proof of concept of Fused Filament Fabrication (FFF) of the Diels-Alder (DA) network polymer, several steps have to be taken. First of all, a printer has to be selected, which needs to fulfil several criteria based on the material characteristics described in Section 2.3. Another step is to create the filament that will be fed to the 3D-printer before being able to print, which was described in Chapter 3. Afterwards the optimal printer settings will have to be determined for this specific material.

4.1 Selection of a 3D-printer

The 3D-printer itself is an important factor and therefore a well-made decision is needed. The printer has to fulfil the following criteria:

Direct (double) extruder A direct extruder with the motor connected to the moving print head is better suited for a flexible filament when compared to a bowden one that has a motor connected to the static printer frame. With a direct extruder, the filament is pulled rather than pushed towards the extruder and moreover, it has a more constrained path, which is needed as flexible materials tend to buckle. Later on, the single extruder will be replaced with a double one to print two materials at once. It is nonetheless good to have a direct single extruder as well for the first testing and to decide the best temperatures, before experimenting with dual extrusion.

Filament size There are two standard filament sizes: 1.75 mm and 2.85 mm. The self-healing (SH) filament will have a diameter of 2.85 mm, as this will make the filament stiffer (thus easier to print), also the tolerances are expected to be better.

Temperature The printer should be able to print at a range of temperatures, at least the range from 50°C-150°C. The gel temperature (T_{gel}) was measured to be around 104 °C (Section 2.3.3) for the current material, and this will be close to the expected printing temperature. Most conventional materials are printed at higher temperatures than this, so being able to print at a high enough temperature is not the problem, but the printer should allow controlled printing at low temperatures as well. Often, 3D-printers are equipped with a cold-extrusion prevention in the software that sets the minimal extrusion temperature

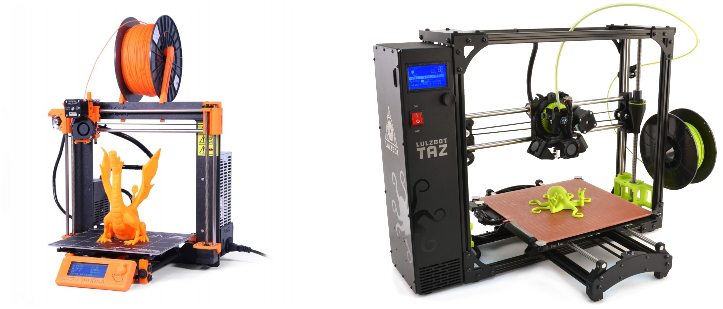
(a) Prusa i3 MK2S (b) LulzBot TAZ 6

Figure 4.1: Two printers that fulfil the requirements, a detailed comparison is needed in order to decide which one is best for the application.
(Source: 4.1a-`shop.prusa3d.com`, 4.1b - `lulzbot.com`)

to above this desired range. Although this lowest printing temperature is not specified by 3D-printer manufacturers, it can be altered in software on most 3D-printers.

Heated bed A heated print bed allows in conventional materials for a better adhesion. For DA materials this heat is needed to control the kinetics of the reaction.

Open source/adaptability Tweaks will almost certainly have to be made to the printer and its control, so it is important to have one where this is easily performed and preferably supported.

Table 4.1 lists a comparison between the most common 3D-printers available at the time of writing. There are four printers in this comparison that have a heated bed and are open source. The Ultimaker 3 and BCN3D Sigma have a dual extruder as a nice advantage, but as they are bowden extruders, they are unfortunately not usable to print the flexible self-healing filament. The Prusa and LulzBot printers (Figure 4.1) already have a direct drive, albeit single extrusion, which is more useful in this case.

The only noticeable differences in this comparison table are the filament diameter and the price. So to make an informed decision, it is needed to look into more detail.

The LulzBot has a larger build volume ($19600\,\text{cm}^3$ vs. $10500\,\text{cm}^3$ for the Prusa) and is heavier. Both have an open frame for easy access. The filament diameter will have to be changed on the Prusa, which is supported. However, this is not very straightforward and it would take engineering time to do the redesign. As it is eventually the goal to have a dual extruder, it is a better option to design this dual extruder instead of a new single one.

The cost of transforming both printers to a dual direct extruder is a consideration between price and ease of use. For the LulzBot, this is rather easy as there is a ‘Dual extruder v3’ tool head available from the manufacturer. The Prusa does not have this, but there is a large community that already developed different extruder designs.

Even though the cost of the Prusa i3 MK2S is lower, the LulzBot is considered a better option as it does standard come with 2.85 mm filament. Moreover, the dual extruder is available from the manufacturer, needing no engineering time to develop one, as is the case with the Prusa.

Table 4.1: Different printers fulfil the criteria; the Prusa i3 MK2S and the LulzBot TAZ 6 will be looked at in more detail.

Name	Prusa i3 MK2S	LulzBot TAZ 6	Zortrax M300	Ultimaker 3	MakerBot Replicator +	BCN3D Sigma
Extruder amount	Single	Single	Single	Dual	Single	Dual
Extruder type	Direct	Direct	Bowden	Bowden	Bowden	Bowden
Extruder change supported	✓	✓	✗	✗	✓	✗
Max. extruder temp. [°C]	300	300	380	260	235	290
Filament diameter [mm]	1.75	3	1.75	3	1.75	3
Open filament	✓	✓	✗	✓	✗	✓
Heated bed	✓	✓	✓	✓	✗	✓
Max. heated bed temp. [°C]	120	120	110	100	N/A	100
Open source	✓	✓	✗	✓	✗	✓
Price [€]	759.50	2110.00	4585.90	2995.00	2072.00	2655.00
Print volume [cm × cm × cm]	$25 \times 21 \times 20$	$28 \times 28 \times 25$	$30 \times 30 \times 30$	$21.5 \times 21.5 \times 20$	$29.5 \times 19.5 \times 16.5$	$21 \times 29.7 \times 21$

4.2 Simulation of the printing process

Before actually trying to print the filament, it is worth doing a few simulations to analyse what will happen to the material during the printing process. Furthermore, these simulations will give a first good estimation of the settings that need to be used to print the SH material.

The simulation is again preceded by a curing time of 24 hours to bring the simulated material in a reference state, as explained in Section 2.2.5 and Section 3.2. The curing of the material will be discussed using the simulated molecular weight: if this is infinite, the material has gelled and a single network extends throughout the macroscopic sample (the software assumes an infinite amount of material available). However, having an infinite molecular weight does not guarantee that the material is in equilibrium, as can be seen by looking at the degrees of conversion. For the printing simulations, the transient behaviour is crucial, as being at equilibrium is only interesting for the starting conditions, so only the molecular weight is looked at in detail here.

As the kinetic simulation software uses a temperature profile $T(t)$, for simulating the kinetics of the printing process itself, the time has to be calculated that the filament is heated before it is extruded in order to get the correct temperature profile. This time depends on various parameters, such as the heater block length l_h and the printing speed v_n and can be estimated as follows.

$$v_f = \frac{d_n^2 v_n}{d_f^2} \qquad \text{(conservation of mass)} \tag{4.1}$$

$$t_h = \frac{l_h}{v_f} \qquad \text{(filament velocity)} \tag{4.2}$$

so that

$$v_n = \frac{l_h \cdot d_f^2}{d_n^2 \cdot t_h} \tag{4.3}$$

where

d_n	nozzle diameter [mm]	v_n	printing velocity [mm/s]
d_f	filament diameter [mm]	v_f	filament velocity [mm/s]
t_h	heat time [s]	l_h	heater block length [mm]

The parameters are illustrated in Figure 4.2. There are parameters that are fixed by the choice of the 3D-printer, such as the nozzle diameter (d_n=0.5 mm), the heater block length (l_h=20 mm) and the filament diameter (d_f=2.85 mm). Note that the nozzle diameter can be changed if desired. As explained in Section 4.3.1, the printing velocity should be low and v_n=5 mm/s is taken. Calculating with these given values, a heat time t_h of 130 s is found.

4.2.1 Printing temperature

To determine the optimal printing temperature, the process is simulated for several printing temperatures. If it is assumed that no heat is added to the filament when it is outside of the heater block, the temperature profile for the simulation is simply a constant temperature for 130 s. In practice, this will not be the case as the filament will heat up gradually undergoing a temperature gradient. The impact of this is not considered in this preliminary simulation.

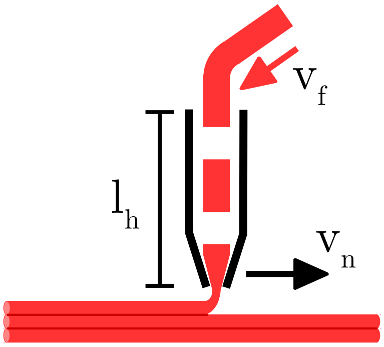

Figure 4.2: Graphical illustration of the parameters needed to calculate the heat time t_h. Due to the diameter reduction in the nozzle, the filament velocity v_f is different from the printing velocity v_n.

The molecular weight of the material is shown as a function of time and at various temperatures in Figure 4.3. Note that as long as the molecular weight is infinite, the material is gelled and flow is very limited or non-existing. At all temperatures, the initially gelled material gradually decomposes, turns liquid at a certain time (degelation), and the molecular weight subsequently decreases to a temperature dependent on the equilibrium value. Very noticeable is the big difference in molecular weight after 130 s, between 110 °C and 115 °C. At such high molecular weights in the order of 5×10^4 g/mol, the material will be too solid to print. Thus, 115 °C is considered to be the lower limit on the printing temperature.

Furthermore, it can be seen that equilibrium is reached sooner when the temperature increases, implying that the higher the printing temperature, the faster can be printed, as less time in the extruder is needed. For each temperature, a slight minimum is reached before going to equilibrium, this allows for a comparison in maximum printing speed. Indeed, when printing faster, the material will not yet be in equilibrium and the too high molecular weight will prevent the material from being extruded. The maximal printing speeds are given in Table 4.2. Even though increasing the temperature from 110 °c to 130 °C allows for the printing velocity to double, these are still very low speeds when compared to conventional soft materials (which are printed around 30 mm/s and up).

One might think that just increasing the temperature would allow for very fast printing velocities, but it has to be kept in mind that irreversible reactions take place at these high temperatures. Moreover, the molecular mass at higher temperatures is lower, meaning that the viscosity will be (much) lower, which might have a negative impact on the print quality. This will have to be tested experimentally.

There are other parameters that could also have a positive impact on the maximum printing velocity. When looking at the parameters directly influencing the printing velocity (Equa-

Table 4.2: Maximum printing velocities at various temperatures. The printing velocities are deduced from the time t_h at which the molecular weight is minimal. The formula $v_n = \frac{l_h \cdot d_f^2}{d_n^2 \cdot t_h}$ is used.

Temperature [°C]	Min. molecular weight [kg/mol]	Max. print speed v_n [mm/s]
110	48.8	5
115	28.0	7
118	22.4	9
120	19.9	10
125	15.6	13
130	12.9	15

tion 4.3), it can be seen that having a longer heater block l_g or smaller nozzle diameter d_n will also be beneficial. Whereas it is possible to exchange the nozzle for a smaller one, having a longer heater block will require to change the whole extruder. Having a smaller nozzle diameter would also mean that the extruded volume over a certain time is lower, and thus a longer printing path is needed, so that the total printing time of a part is not necessarily lower. Another possible enhancement is to have the printer positioned inside a heated environment. If the filament is pre-heated instead of being at room temperature, the heating and degelation will happen faster, and thus the maximum printing velocity is increased.

4.2.2 Heated bed - heated environment

The simulation of the influence of a heated bed and of the environment temperatures are actually the same: the temperature is lowered after printing and kept constant. The difference here is that the simulation is only valid for the first few printing layers when only a heated bed is considered. Above these layers, the temperature of the material gradually decreases to the environment temperature. With a heated environment, all layers are at the same temperature and the simulation is valid for the whole part. Although the printer is not equipped with a heated chamber, as the simulation is the same as for the heated bed, the impact of having one can easily be deducted.

The simulation is performed after having the 24 hour curing time at room temperature and $t_h = 95\,\mathrm{s}$ of printing. This is equal to having a v_n of 6.84 mm/s, which is slightly below the maximum printing velocity $v_n = 7\,\mathrm{mm/s}$ (calculated via Equation 4.3) for the lowest temperature considered (115 °, data taken from Table 4.2). Afterwards, the temperature is set constant, mimicking the heated bed/environment. This simulation is executed for printing temperatures between 115 °C and 120 °C, while the heated bed is simulated for several temperatures ranging from room temperature to 100 °C.

When looking at the result shown in Figure 4.4, it is clear that at higher temperatures of the heated bed, the gelation (molecular mass becoming infinite) happens faster after the printing

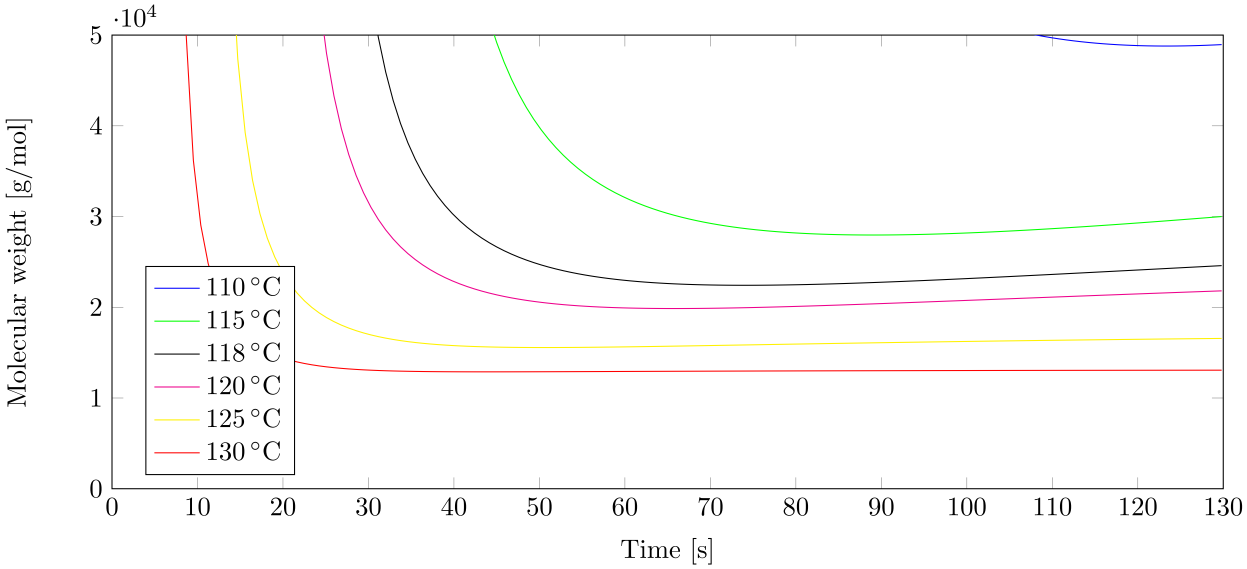

Figure 4.3: Simulations of the change in molecular weight during the printing on various temperatures allow to see that the SH material should not be printed below 115 °C.

(note that the origin of the time axis is placed at the moment of extrusion, so right after the printing). This time to gelation not only depends on the heated bed temperature, but also on the temperature of the printing itself. In Figure 4.5 can be seen that a lower printing temperature is beneficial to achieve a lower time to gelation. This time to gelation is an important parameter for several reasons. First of all, this will impact how long a layer takes to adhere to the previous layers. If a new layer is printed over the previous one, while this previous layer is not yet gelled, the print quality will be negatively impacted as the shape of the previous layer (which has still a lot of mobility) will be distorted by the new one. With this insight, it can be stated that the time to gelation is a lower limit on the time per layer, which can be set in the software. It is also considered the main limit on the printing speed, as in theory, the printing velocity v_n can be increased as much as needed by altering the printer (increasing l_h), but the kinetics of gelation cannot be faster than just below $\mathrm{T_{gel}}$.

A second reason why the time to gelation is interesting, is how long the print will need to be on the print bed (after the part is finished) before it can be taken off. Once the material gelled, the temperature can be set to room temperature and left to cool down. Cooling down is important as the advancing network formation and increasing storage modulus allows for easier removal of the part. Moreover a human would risk getting injured trying to remove the part from the hot print bed.

Another factor to consider is that electronics have a working range that will limit their operation temperature when working with a heated environment. For consumer electronics, the limit is often taken as 70 °C. Also the material of which the printer is made can limit the environment temperature. This depends of course on the material itself, but many printers are partially made from PLA ($\mathrm{T_g}\approx$60 °C) or ABS ($\mathrm{T_g}\approx$105 °C), which should not be used above their $\mathrm{T_g}$ to keep their strength and shape.

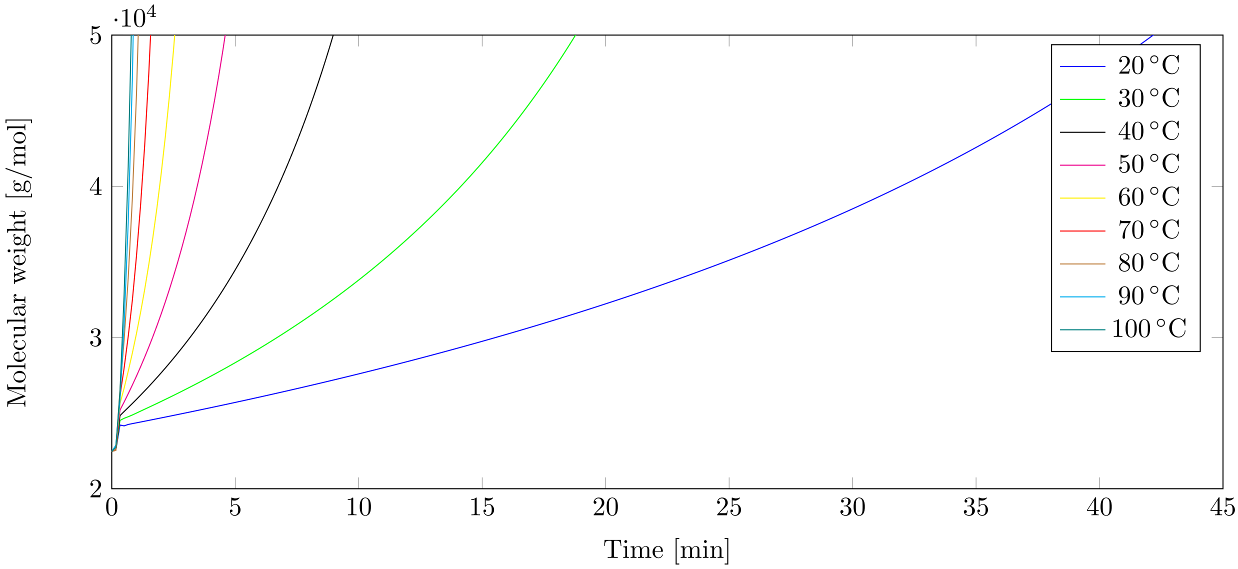

Figure 4.4: The heated bed temperature has a large influence on the time to gelation. This time should be as short as possible to prevent the material from flowing.

In conclusion, as the printer is currently not equipped with a heated environment, the heated bed temperature could be set to 70-80 °C. Going higher in temperature is not beneficial enough, also considering the increased flexibility of the SH material at these elevated temperatures.

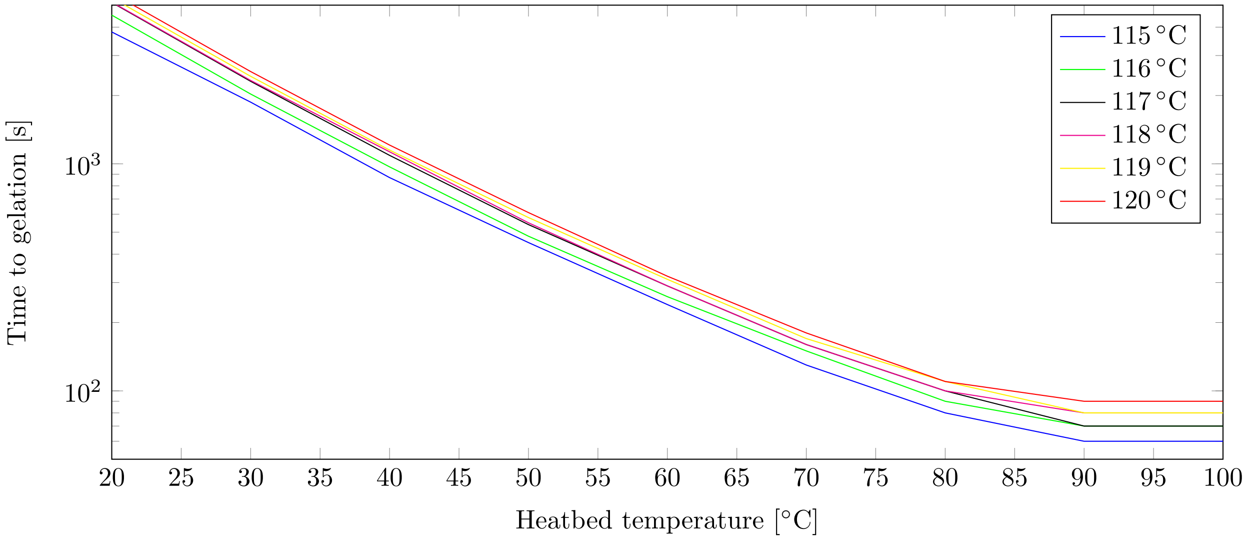

Figure 4.5: The time to gelation depends on the printing temperature and the heatbed temperature. Simulation done in steps of 10 s.

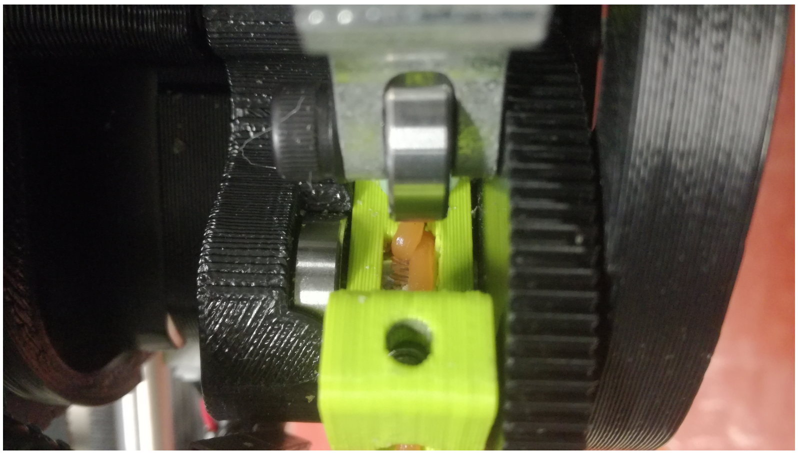

Figure 4.6: Buckling under the metal hobbed gear is to be avoided: the filament gets stuck between the gear and its green plastic housing, which leads to failed prints.

4.3 Practical 3D-printing

The JT5000 polymer that is extruded in filament form, can be loaded into the 3D-printer. As this is a new material to be printed, all settings and optimal conditions have to be determined. This will be performed by looking at the results of the simulations developed in Section 4.2 and finetuning them. These simulations have shown that the material should not be printed below 115 °C and that 80 °C is a good temperature for the heated bed.

4.3.1 Feeding the filament

With its Young's modulus of 6.4 MPa, the material is more flexible than the flexible filaments currently on the market. Of those materials, the thermoplastic polyurethane NinjaFlex has the lowest Young's modulus (12 MPa) [45]. Due to this very low modulus, the filament is prone to buckling. This buckling leads to jamming of the extruder and thus to a failed print. Three ways of buckling and jamming were observed.

- Buckling in the extruder path. If the diameter of the filament is too thin, there is enough room for it to buckle, bend and twist within its constrained path, which has a diameter of around 3.1 mm. This is only noticeable in the print quality as the extruder does not extrude the amount of material that it is supposed to.
- Buckling under the hobbed gear (see Figure 4.6). The soft filament is pulled in between the hobbed gear and the housing surrounding it. When the gear drives even further, it grinds through the filament, breaking it in two parts.
- If the filament diameter is larger than 3.1 mm, it does not fit in the extruder, jamming it.

From these problems, it becomes once again clear that a consistent filament diameter between 2.85 mm and 3 mm is very important and a lot of improvements for the printing can be realized by improving the filament. The buckling phenomenon can also be reduced by considering the buckling equation (Euler's critical load).

$$L_B = \frac{\pi d_f}{4}\sqrt{\frac{E}{P_B}} \tag{4.4}$$

where

L_B Maximum length of the filament before it will buckle

d_f Filament diameter

E Young's modulus

P_B Pressure applied on the filament

Note that buckling is largely prevented by having a constrained path, so that there is no space for the filament to buckle. In the small areas where the path is less constrained (such as directly after the hobbed gear), the maximum length of the unconstrained part is L_B. In Equation 4.4, the diameter of the filament is an important parameter, which is also a reason that 2.85 mm filament is preferred over a 1.75 mm one. The modulus of elasticity is a given for the material.

Finally, the buckling depends on the load, which can be divided in friction and pressure. The friction is difficult to change as it depends on both the DA material and the materials the extruder is made of. The force needed to push the material through the hot-end can be lowered by several factors.

- Lower the flow rate of the material, which is equivalent by lowering the printing velocity.
- Increase the temperature to lower the viscosity.
- Use a larger nozzle diameter so the pressure needed to push material through at a certain flow rate is lower.

The nozzle preinstalled on the extruder is 0.5 mm, which is already quite large. The larger the nozzle, the less details can be printed, so opting for an even larger nozzle diameter is not preferred. In Section 2.3.1, it was determined that the material starts to degrade at 200 °C, but even at temperatures above 120 °C, irreversible reactions were observed, as described by Terryn et al., so this will be considered the maximum allowed temperature [1]. This leaves the printing velocity as the easiest parameter to impact the pressure in the nozzle. A velocity of 5 mm/s was used to print the first samples. A low printing velocity is also beneficial because the material is heated for a longer period.

4.3.2 Temperature settings

Extruder temperature

From the simulation, it is expected that the printing temperature should not go below 115 °C, but the optimum extruder temperature is determined experimentally by printing the same object at different temperatures (Figure 4.7). This experiment shows that lower temperatures give a better quality print. At 120 °C and 125 °C, it can be seen that the material flowed before gelation and all detail is lost. At 117 °C, this does not notably happen, leaving the details intact and resulting in a better dimensional accuracy. At temperatures lower than 117 °C, the material was unable to flow consistently out of the nozzle, and no satisfactory samples were obtained. The printing temperature is chosen to be 117 °C.

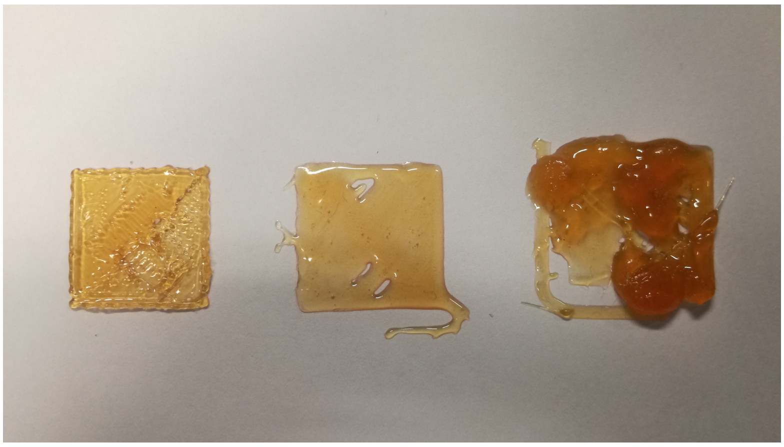

Figure 4.7: A test specimen of 20 mm×20 mm printed at different extruder temperatures: 117 °C (left), 120 °C (centre), 125 °C (right). A better print quality is achieved at low temperatures. Note that the number of layers printed is not equal in the different samples, due to the filament buckling. The print at 125 °C is above the allowed temperature, but is added for comparison purposes.

Heatbed temperature

The heatbed has a Polyetherimide (PEI) surface and the temperature can be regulated between the environment temperature and 120 °C. In FFF, this heatbed serves several purposes. First, heating increases the surface energy, which allows for a better adhesion of the print to the heated bed. Secondly, the heated bed can also prevent warping. When a layer of hot material is deposited onto a layer of cooled material, large stresses can develop in the previous (compression) and in the new layer (tension) once the material gelled, as the hot network cools further and contracts. This can be prevented by keeping the lower layers warm.

The heatbed adhesion proved to be sufficient: the SH material sticks well enough to the PEI surface. As the simulation showed that setting the heatbed temperature to 90 °C allows for faster gelation, this temperature is thus used. It is difficult to verify the simulations experimentally, but it is noticed that the parts can be removed from the printbed faster when setting the heatbed to higher temperatures.

4.4 Print quality

Generally the print quality depends on a lot of factors. In first instance, it depends on the printer itself and the material that is being printed, but it also depends a lot on the settings of the software. The software of choice is Cura LulzBot Edition, and the settings that are eventually used are given in Appendix C. Although quantifying the quality is useful for comparison, to objectively measure the print quality is not always easy as it is often only visual. To give an overview of the print quality achieved, the classification of Ko et al. is followed [46]. There are two categories within the quality assessment: dimensional accuracy and surface finish, which they also link to the build time. This is because a slower printed part has more potential quality. An easy example of this is that reducing the layer height increases the build time significantly, but also improves the surface quality in the vertical direction. However, in this analysis, the print time is not considered.

4.4.1 Dimensional accuracy

Dimensional accuracy can be seen as the comparison of the dimensions of the digital 3D-model and the printed part. Measuring is easily performed with a calliper. A big part of the dimensional accuracy is determined by the printer calibration, which was performed at the factory.

The 20 mm×20 mm squares that are shown in Figure 4.7, are used to see whether printing with the SH material also allows for a good accuracy. Measuring eight of these squares in both directions gives a mean error of 0.2 mm with a standard deviation of 0.4 mm dimensional error. This shows that improvement is still possible but these results are already very good.

Printing an overhang or a bridge (printing on air, with no material underneath) also has to be considered when looking at dimensional accuracy. For conventional materials, this can be achieved by lowering the printing speed or temperature (to increase the viscosity of the material) and cooling extensively so that the material hardens as fast as possible. When working with DA materials, extensive cooling slows the kinetics down and increases the time it needs to cure. When looking at Figure 4.4 and Figure 4.5, it can be seen that having gelation within a few seconds is not feasible for this material within a reasonable temperature range. It can thus be concluded that printing overhang or bridging is currently not possible.

Being unable to print an overhang is not necessarily a problem. Instead, when a part requires overhang to be printed, support material can be used to print on so that the DA material does not have to be printed on air. As support material, typically polyvinyl alcohol (PVA) is used because it is water soluble, while the DA network is not. Also PLA or ABS can work and provide a cheaper option. Printing with support has however not yet been tested, but adhesion to the support material will be critical.

Another problem that occurs, is surface tension. When printing, and certainly at a higher temperature, the top surface typically becomes convex. This poses a big limitation on the printing process. When printing a beam, for example, at each layer the surface becomes slightly convex. This means that at the sides, there is a small band on the original surface where there is no longer material. As the printing of overhang is impossible, this means that there will only be material deposited on this reduced surface. Eventually, instead of having a rectangular cross section, it becomes trapezoidal as the outer walls are leaning towards each other. This limits the printing height of the part. This effect can be reduced significantly by lowering the printing temperature, as can be seen on Figure 4.7 or increasing the heated bed temperature. In the centre sample, the sides are convex, whereas in the leftmost sample, this effect is limited, though still existing.

4.4.2 Surface finish

When speaking about surface finish, actually different types of surfaces have to be discussed separately: the bottom, the top and the side surfaces.

The bottom surface is printed directly on the PEI heated printbed. This gives a macroscopically flat surface since the printbed adhesion is perfect. Due to the surface roughness of the

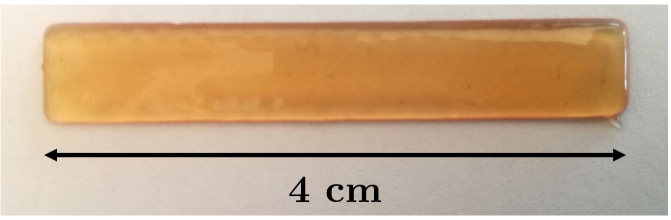

Figure 4.8: A printed sample in JT5000. Almost no texture from the layers is present.

printbed, the bottom surface has a matt look.

The top surface is, as discussed previously, slightly convex due to the surface tension. One important thing to notice here is that there is almost no texture from the filament strands (Figure 4.8). When printing with conventional polymers, lines showing the extruder (print head) movement are clearly visible. Due to the SH property of the material and the relatively slow kinetics, these lines are smoothed out right after printing. This is an advantage compared to conventional materials: no post-treatment is needed to increase the visual appeal.

The side surfaces normally also consist of clearly identifiable horizontal layers, which are healed together when printing with SH material. Besides the visual advantage, this also has structural advantages. First of all, it makes the part airtight, which is very difficult to achieve using conventional materials. A second advantage is explained in Section 4.5.1: the printed material does not have anisotropy by printing and its full mechanical properties can be exploited. This is also not the case with conventional materials used in 3D-printing [47]. Another observation is the presence of small bubbles inside the printed part, especially when printing at higher temperatures. These bubbles are most probably due to evaporation of water or remains of solvent (as shown in Section 2.3.1), so the materials should be stored clean and dry. This might have a (small) influence on the mechanical strength of the material, but they are to be avoided mainly because they can potentially lead to air leaks in future printed soft actuators. To overcome this, treatments could be developed in the future to further improve the aesthetic and mechanical properties.

4.5 Material properties

After printing, it is important to verify the properties of the printed material. After producing the filament and printing, the material has at least gone through two heat cycles and this has potentially created irreversible bonds. To test this, material samples are printed, which can be compared to the original results from Section 2.3. Note that no samples can be made directly from the filament due to the shape.

A first test is done using a rheometer, the T_{gel} of the printed material is determined at 114 °C (see Figure 4.9). It is seen that the T_{gel} is higher compared to the original material (T_{gel}=105 °C), determined in Section 2.3.3. The change is due to irreversible bonds that were formed during the filament extrusion and printing process. Due to this higher T_{gel}, the filament extrusion temperature and printing temperature need to be set higher in the next production cycle. Note that the material that is tested, did go through several recycling cycles, so the actual

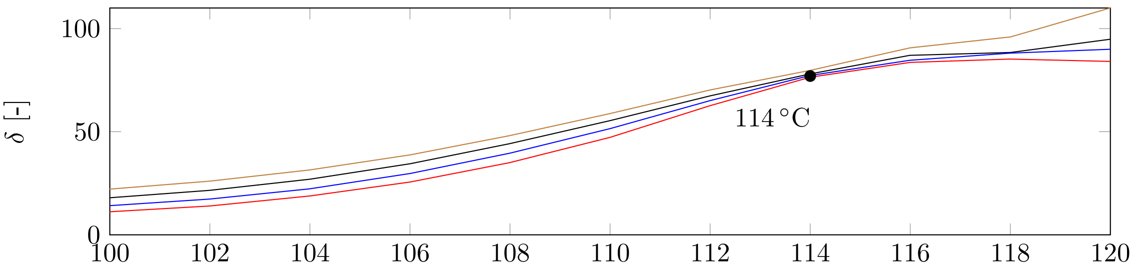

Figure 4.9: The rheometric analysis of the printed JT5000 was done at various angular velocities ranging from 1.99 rad/s to 19.87 rad/s, depicted as different colours. T_{gel} is determined as 114 °C.

influence per cycle is probably lower.

A Dynamic Mechanical Analysis (DMA) analysis is also performed on the printed samples, see Figure 4.10. The printed sample is compared to a reference sample that was stored under the same conditions at 30 °C. The samples are however not taken from the same batch of DA material, which can cause small differences. The T_g has increased with 2 °C, which is acceptable and a possible explanation is the difference in batch. In general, the characteristics of the printed material are close to the reference sample, which shows that the printing process does not alter the material properties significantly.

4.5.1 Isotropy

Printing conventional polymers introduces anisotropy in the material due to the layering in the Z-direction [47]. This means that the part orientation in the printing process is important for the mechanical behaviour of the final object. Due to the SH property of the DA materials, it is expected that this anisotropy is not present. To test this, samples were printed in different directions and compared. The angle of the direction is defined as the angle between the pulling force and the direction of the strands that were printed.

The standard setting is to print each layer alternately in +45 ° and -45 ° to remove as much anisotropy in the plane as possible. This is compared with samples printed only in the 0 ° and 90 ° directions, to see the influence in case anisotropy is maximized. A comparison is made in Table 4.3. For a printing direction of 90 °, so perpendicular to the applied force, a small loss in fracture strain and ultimate tensile strength is noticed. This is most probably due to small notches in the samples at the sides where a crack can be initiated more easily (at a lower overall stress). In the 0 ° direction, no apparent loss in mechanical properties is noticed. There is also a larger variance noticeable in the unidirectional samples. A possible explanation is that the surface of these samples is not flat enough. As in these samples, the strands of filaments are printed on the same position each layer, small gaps are present in between which can cause small stress concentrations. Overall, it is possible to confirm that the anisotropy present in printed SH parts is very limited.

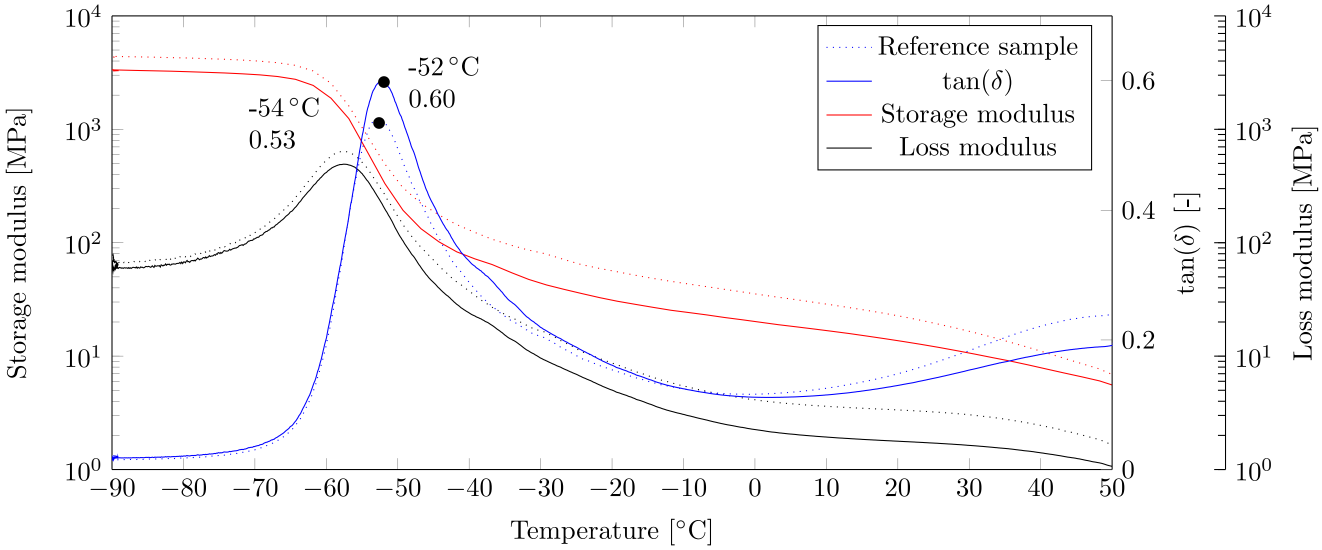

Figure 4.10: DMA analysis of a printed sample (JT5000) shows a T_g of -52 °C. A reference sample stored under equal conditions shows a T_g of -54 °C. Measurement performed with an oscillatory strain of 0.5 %, static force of 0.01 N, 125 % force tracking, and a temperature ramp of 2.50 °C/min.

Table 4.3: Comparison of the measured mechanical properties in different printing orientations. The detailed measurements are given in Appendix D.

Sample	Ultimate tensile strength [MPa]	Fracture strain [%]	Young's modulus [MPa]
Standard print pattern	1.6±0.2	108±5	5.8±0.6
90 ° direction	1.4±0.1	91±34	5.3±1.0
0 ° direction	1.6±0.2	108±21	6.2±1.1

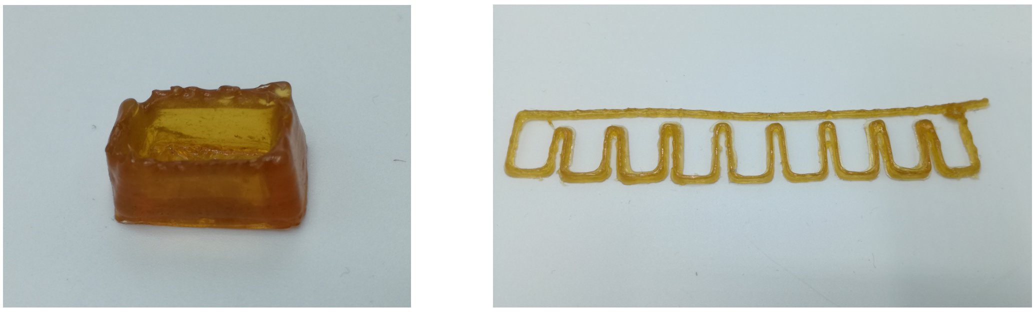

(a) (b)

Figure 4.11: Two proofs of concept were printed for soft inflatable elastic robotic actuators. (a) A cell of the gripper and hand as shown in Figure 1.2. (b) A new design for a SH actuator, a sheet on top and below should be added to finalize the design.

4.6 Conclusion

The developed printing process has successfully shown its potential, although the printed parts might have extra irreversible bonds, this does not change their mechanical properties. The printed parts have a very good surface finishing, which allowed to print proofs of concept for robotic actuators, as shown in Figure 4.11. Due to some irregularities still present in the filament, the filament buckles and jams sometimes. When this happens, the printing process has to be stopped. This happened as well during the printing of both parts in Figure 4.11, which is the reason why they are not fully finished. Nevertheless, they fully show the potential of the FFF process for SH DA polymer networks. Together with this, challenges such as printing overhang or with support remain and will be researched in future work.

Chapter 5

Towards multi-material printing

Printing multiple Diels-Alder (DA) materials in for constructing an actuator gives more design freedom. More complex actuators can be developed since multi-material printing of materials having different storage moduli allows to create anisotropic deformations, which can be used to develop actuation motions [3]. To study the feasibility, first the interface between two DA materials is studied. Afterwards a second material is proposed to extrude into filament and printed.

5.1 Study of the interface between JT5000 and JD4000

The interface between different DA materials is studied to see how well the joining method of healing one onto another compares to glueing. During this study, materials JT5000 and JD4000 are used as they have comparable Young's moduli (E_{JT5000}=6.4 MPa, Section 2.3.2; E_{JD4000}=5.1 MPa, [1]). JT5000 is the material that was used for filament extrusion and printing. JD4000 is in these samples prepared with a black colour additive, as shown in Figure 5.1. Different samples are compared:

- Healed for 60 minutes at 80 °C
- Healed for 60 minutes at 90 °C
- Glued with Pattex Multi[1]

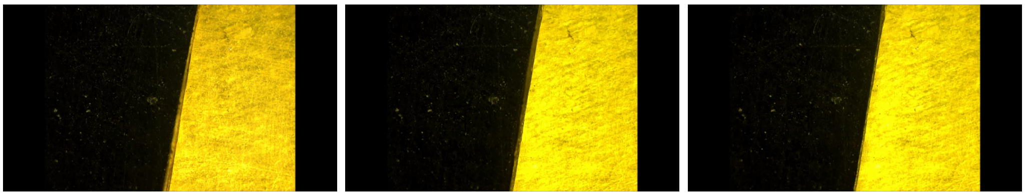

Figure 5.1: Microscopic images of the healing of JD4000 (black) and JT5000 (yellow) from left to right.

---

[1] Datasheet available on: `https://images.obi.de/PROD/AT/document/973/973072_datasheet_1.pdf`

Table 5.1: Comparison of the measured mechanical properties at the interface of two DA materials.

Sample	Ultimate tensile strength [MPa]	Fracture strain [%]
Glued	0.3±0.1	43±24
Healed at 80 °C	1.0±0.3	144±76
Healed at 90 °C	1.1±0.1	237±26

On each of those samples, a stress-strain test until fracture is performed to determine the ultimate tensile strength and fracture strain. A comparison of the obtained results is given in Table 5.1, the full plots are given in Appendix E. Looking at the data, it becomes clear that healing is more effective as a joining method than using glue. The glued samples have an ultimate tensile strength that is only 20 % of the samples healed at 90 °C, and the fracture strain is even more problematic. When comparing the samples healed at different temperatures, it is seen that the tensile strength is similar, but that the fracture strain increased when healing at higher temperatures. The fact that one of the samples healed at 80 °C failed at a similar strain as the samples healed at 90 °C might indicate that the difference comes from misalignment at the interface rather than from intrinsic differences of the interface after healing. In other words, healing at higher temperatures is beneficial as misalignments are smoothed out and more predictable results are obtained. The glued samples show a very large variance, making it difficult to predict the maximal operating range of the eventual actuator. This shows that dual material printing can indeed be an effective method to produce multi-material parts and is worth developing.

5.2 Developing the process for other Diels-Alder materials

To be able to print multiple materials, the whole process of looking for optimal filament extrusion and printing conditions should be redone for each DA material. Luckily, most of the developed concepts and solutions can be transferred to new materials. As a second material, JT3000 is chosen in a non-stoichiometric ratio ($r = 0.5$) of DPBM over furan-functionalized Jeffamine to increase the flexibility compared to stoichiometric JT3000. This material is prepared with indigo as colour additive ($C_{16}H_{10}N_2O_2$) giving it a blue/green colour to ease the distinguishing from the JT5000 material that was always prepared without colour additives.

Extruding the filament did require other temperature settings, and obtaining them was just a matter of trial and error. For every DA material, these settings will have to be tuned slightly as they depend on the gel temperature (T_{gel}). For the JT3000 material used, the T_{gel} is higher and therefore, the extrusion (and printing) temperature settings are also higher.

Pre-heater	128 °C	**Motor speed**	1 rpm
Heater	118 °C	**Fan**	off

A sample of filament is shown in Figure 5.2. The quality is comparable with that of the JT5000 filament, and again slight sharkskin is still present. A disadvantage of this material is that it is

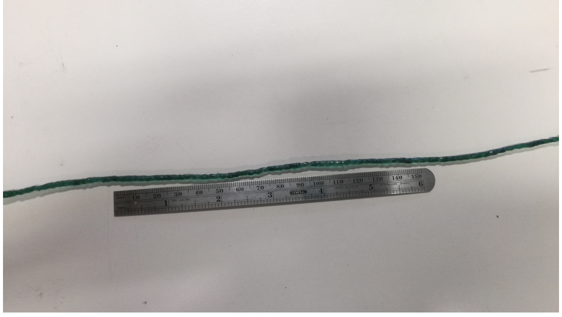

Figure 5.2: Filament produced from JT5000 with stoichiometric ratio $r = 0.5$.

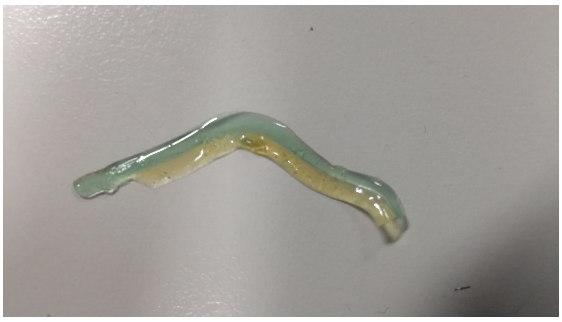

Figure 5.3: A small piece of a multi-material print is successfully obtained. JT5000 (yellow) and JT3000 (blue/green) are printed next to each other.

more sticky, due to the open bonds resulting from the excess of furan-functionalized Jeffamine. This increased the friction of the filament in its confinement and made the printing process very difficult. Nevertheless, several small parts were successfully printed and a first attempt towards multi-material printing was made. No full samples were obtained that could be tested, but a small printed piece is shown in Figure 5.3. This proves that it is certainly possible to do this, but more research is needed.

5.3 Conclusion

In this chapter, it has been proven that healing different DA materials to each other gives better mechanical properties compared to glueing. This ais an important reason for evaluating the feasibility of dual-material printing. Extruding the filament did not pose any serious problems, but printing the second material proved significantly more difficult. More research and technological development is needed to improve this process and to select other DA materials that are suited for printing. Nevertheless, it has been proven possible to print multiple materials next to each other.

Chapter 6

Conclusion and future work

6.1 Conclusion

In this research the goal was to create a proof of concept for a platform that allows the Fused Filament Fabrication (FFF) or so called 3D-printing of self-healing (SH) Diels-Alder (DA) polymer networks. In order to do this, the problem is divided into two subtasks, being the filament extrusion and the 3D-printing itself.

Extruding the filament proved a difficult task where a slight change in parameters has a big influence on the filament quality. During extrusion, different failure phenomena are observed of which sharkskin is the most prominent and problematic. To overcome these problems, different solutions (optimized die design, reduced extrusion velocity, and grinding) are implemented, which reduced the phenomena significantly. At this point, the filament is considered good enough to be used for 3D-printing, but it is still not perfect. Small irregularities on the surface remain and over the range of a few centimetres, the diameter may vary with a tenth of a millimetre as well.

The results of the 3D-printing depend largely on the quality of the filament. If it is too thick, it will not fit, and if it is too thin, the filament will buckle and be damaged easily. When the filament is of good quality, the 3D-printing works and even multiple materials could be printed. Several test samples for material analysis were printed and even a small conceptual actuator with fine details was made. This shows that there is a lot of potential for additive manufacturing using these DA materials. The printing height of the shapes that are currently feasible is limited. By adding a heated chamber around the printer, this problem will most likely be solved. Also printing overhang is currently not possible due to the low viscosity of the DA material when exiting the nozzle.

Research was also performed to prepare multi-material prints: a second material was printed next to a first one and an attempt was made to produce multi-material parts. A small printed part showed that this is feasible. This is the onset for further research in this field, as it was proven that healing multiple materials to each other gives better mechanical properties compared to glueing.

In general, this proof of concept shows that it is certainly possible to 3D-print different DA materials and that this technique can already be applied to manufacture small and simple parts without loss of mechanical properties. To reliably print bigger and complexer parts, filament quality and filament-handling in the printer need further improvement, but this work forms a solid basis to start from.

6.2 Future work

For further improvement of the printing process, there are several options that should be considered. Using a filament extruder equipped with multiple heating zones and an optical sensor that allows for diameter control will have a positive impact on the filament quality. A heated chamber can be implemented to improve the quality and achievable complexity of the parts that can be printed. The simulations for this were executed during this research and showed great potential. Also, experiments should be performed to see whether the limitation of printing overhang can be resolved by printing with a (to be selected) support material.

These adaptations should allow for a full-scale working actuator to be printed and tested. This can be compared to an actuator made using other manufacturing techniques, although it is expected that the performance is equal. Furthermore, a larger variation of DA materials can be extruded into filaments and printed. One interesting example, is to print a DA network with a glass transition temperature (T_g) above room temperature. This will allow for actuator designs in which multiple materials having markedly different mechanical properties are printed at the same time.

For this multi-material printing, a first step is to verify that the printed parts have the same mechanical properties as the non-printed parts. Next, an actuator can be designed that is printed using different DA materials that bend due to the inherent anisotropy introduced in this way.

Another idea that is being considered, is to implement an electrically conductive DA material in the actuator that will function as a sensor (e.g., by a changing resistance resulting from deformation or damage). With dual material printing, adding this conductive material in the design will become feasible. In this way, future self-healing robots might be able to sense displacement and force, and moreover, they will be able to heal themselves when needed.

Also other additive manufacturing methods could be studied. Together with the research group SMaRT of KULeuven, Selective Laser Sintering (SLS) will be evaluated, for which the material should be in powder form. This research has already proven that producing powder does not influence the mechanical properties of the material.

Regardless from the SH property, the developed proof of concept of reactive printing allows for a better surface finishing of 3D-printed parts and diminishing of the anisotropy. Although it is currently developed in the frame of soft robotics, this technology can find applications in other fields where the 3D-printing of self-healing structures can be interesting, such that the developed platform could have a much broader economical potential in the future.

Appendices

Appendix A

Synthesis reaction of the Diels-Alder material

The synthesis starts from the three reactants given in Figure A.1

- A Jeffamine D- or T-series, obtained from Huntsman.
- Furfuryl Glycidyl Ether (FGE, 96 %), obtained from Sigma-Aldrich.
- 1,1'-(methylenedi-1,4-phenylene)bismaleimide (DPBM, 95 %), obtained from Sigma-Aldrich.

and consists of four steps

1. A Jeffamine D- or T-series is combined with FGE in stoichiometric ratio to react to a furan-functionalized compound (Jx-FGE) through an epoxy-amine reaction (Figure A.2). This reaction is performed at 60 °C for a week while stirring, the reaction is finished by heating to 90 °C for 2 days.
2. The furan-functionalized compound (Jx-FGE) is combined with 1,1'-(methylenedi-1,4-phenylene)bismaleimide (DPBM), whether or not in stoichiometric ratio $r = \frac{n_{\text{Maleimide}}}{n_{\text{Furan}}}$. This mixture is dissolved in chloroform and stirred for 24 hours at room temperature (Figure A.3).
3. Hydroquinone is added to the solution as a radical inhibitor to avoid the formation of irreversible bonds above 120 °C.
4. The solution is poured in teflon moulds and placed in a vacuum at 90 °C for 24 hours until all chloroform is evaporated.

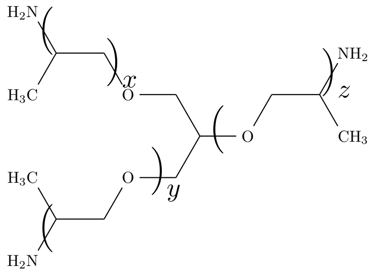
H_2N
x
NH_2
H_3C
O
z
O
CH_3
H_3C
O
y
H_2N

(a) Jeffamine T-series

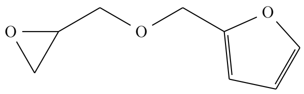

(b) Furfuryl Glycidyl Ether (FGE)

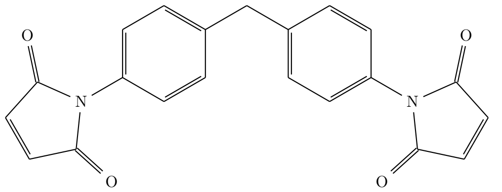

(c) 1,1'-(methylenedi-1,4-phenylene)bismaleimide (DPBM)

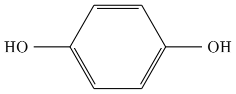

(d) Hydroquinone

Figure A.1: The three reactants and the radical inhibitor hydroquinone are used in the synthesis.

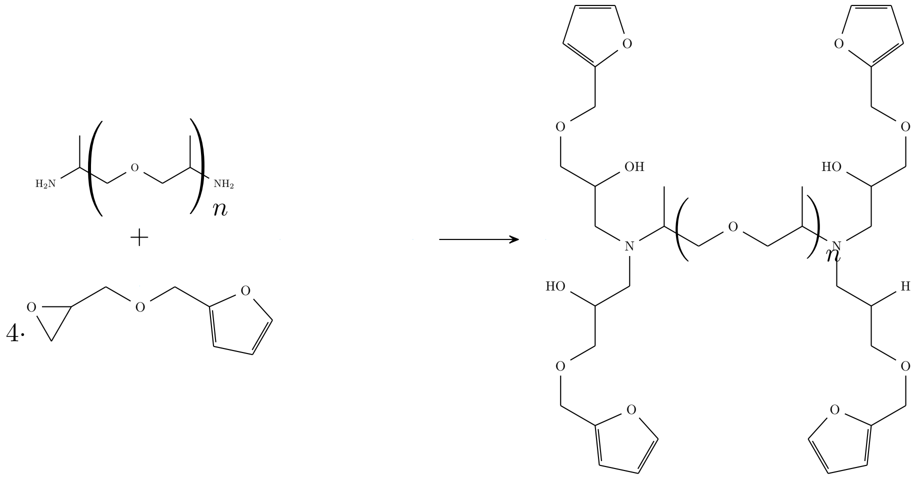

Figure A.2: Combining a Jeffamine with FGE to obtain a furan-functionalized compound.

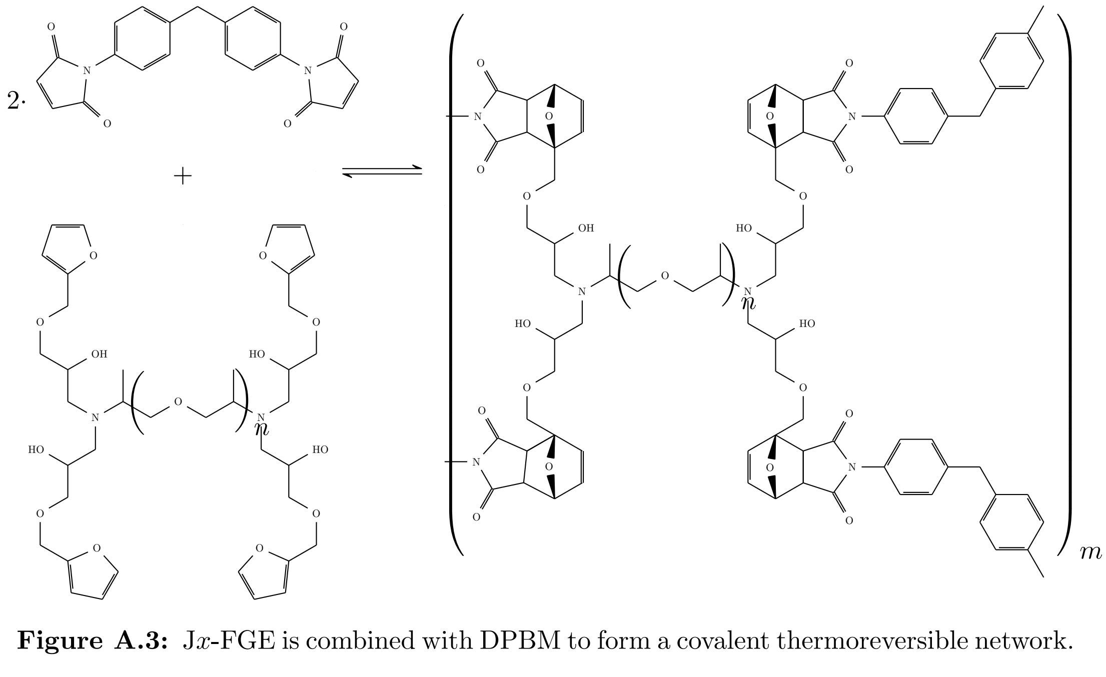

Figure A.3: Jx-FGE is combined with DPBM to form a covalent thermoreversible network.

Appendix B

Adaptations to the filament extruder

To be able to lower the extrusion velocity, the Noztek is partly disassembled and adapted using extra hardware and software. A schematic is given in Figure B.1. An H-bridge shield is used to connect the motor to the Arduino UNO and control it. The H-bridge (Infineon DC motor control shield with BTN8982) is fed using the internal 24 V power source of the Noztek Touch, while the Arduino is fed using a USB-power plug.

The rotary encoder is disconnected from the machine internals and its signals are redirected to the Arduino. The motor power source is also disconnected and attached to the H-bridge shield. The H-bridge is equipped with two half-bridges which can be used as a full-bridge if desired. As the extruder should only turn in one direction, ony a half-bridge is used. The Arduino is programmed with a PID control to keep a regulated rotational velocity which can be set by turning the potentiometer.

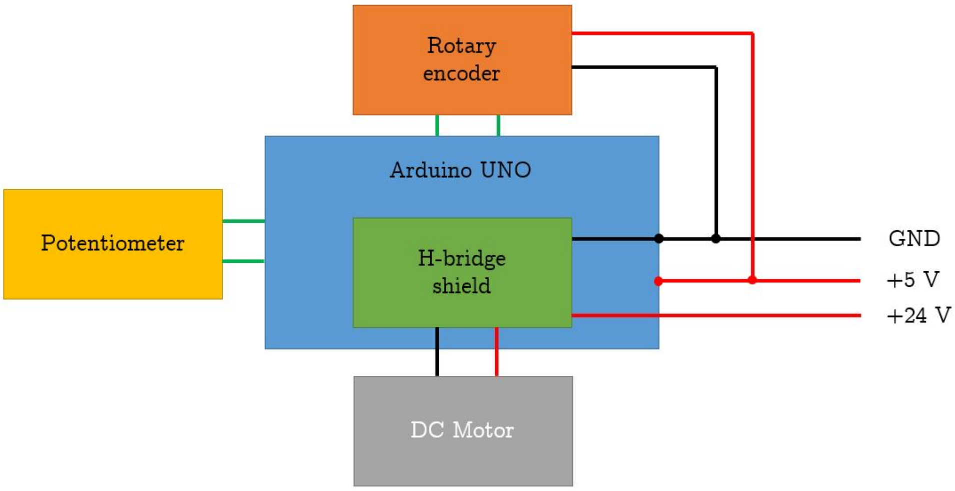

Figure B.1: Schematic drawing of the H-bridge set-up used to control the motor velocity.

Appendix C

Printer settings

The printer software Cura LulzBot editionallows to set various parameters for the printing process, the settings that were used are described here using the export function.

```
    version = 2
name = Self-healing
definition = lulzbot_taz6_dual_v3

    [metadata]
type = quality_changes
quality_type = custom
setting_version = 1

    [values]
adhesion_extruder_nr = 0
adhesion_type = skirt
cool_fan_full_at_height = 0
cool_fan_full_layer = 1
cool_fan_speed = 60.0
cool_fan_speed_0 = 60
cool_fan_speed_max = 100.0
cool_min_layer_time = 60
cool_min_layer_time_fan_speed_max = 120
default_material_print_temperature = 117
material_bed_temperature = 90
material_bed_temperature_layer_0 = 90
material_diameter = 2.85
material_final_print_temperature = 117
material_flow_layer_0 = 100
material_initial_print_temperature = 117
material_keep_part_removal_temperature = False
material_part_removal_temperature = 0
material_print_temperature = 117
material_print_temperature_layer_0 = 117
material_probe_temperature = 80
material_standby_temperature = 110.0
prime_tower_enable = False
retract_at_layer_change = False
retraction_amount = 0
retraction_enable = False
retraction_speed = 10
speed_infill = 5
speed_layer_0 = 5
speed_print = 5
speed_topbottom = 5
speed_travel = 30
speed_wall_0 = 5
speed_wall_x = 5
support_enable = False
switch_extruder_retraction_amount = 0
switch_extruder_retraction_speeds = 10
```

Appendix D

Isotropic tensile tests

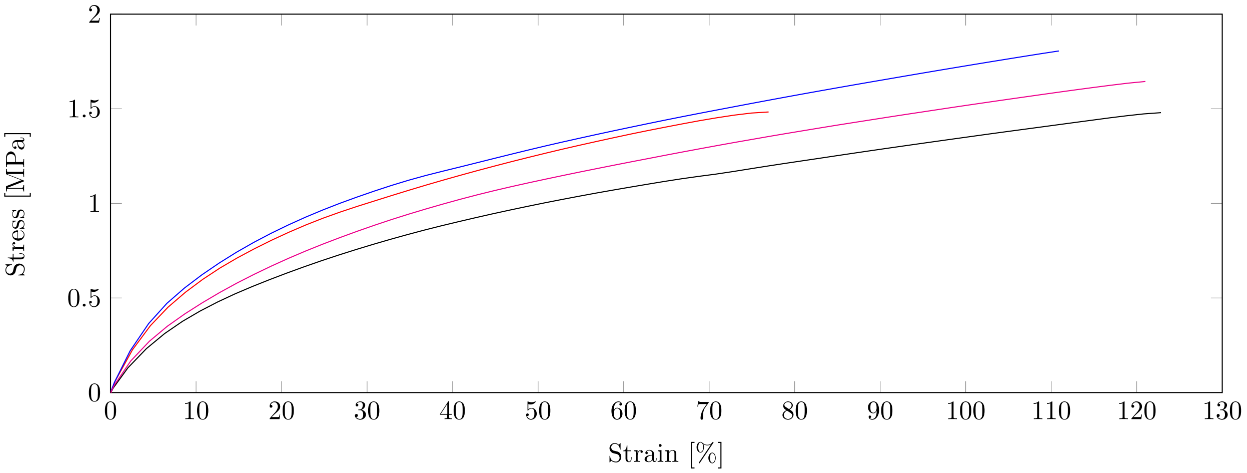

Figure D.1: Stress-strain curves of printed samples JT5000 in the 0 ° direction. Four samples were tested at a strain rate of 60 %/min at an ambient temperature of 25 °C. The ultimate tensile strength is 1.6±0.2 MPa at a strain of 108±21 %. The Young's modulus is 6.2±1.1 MPa.

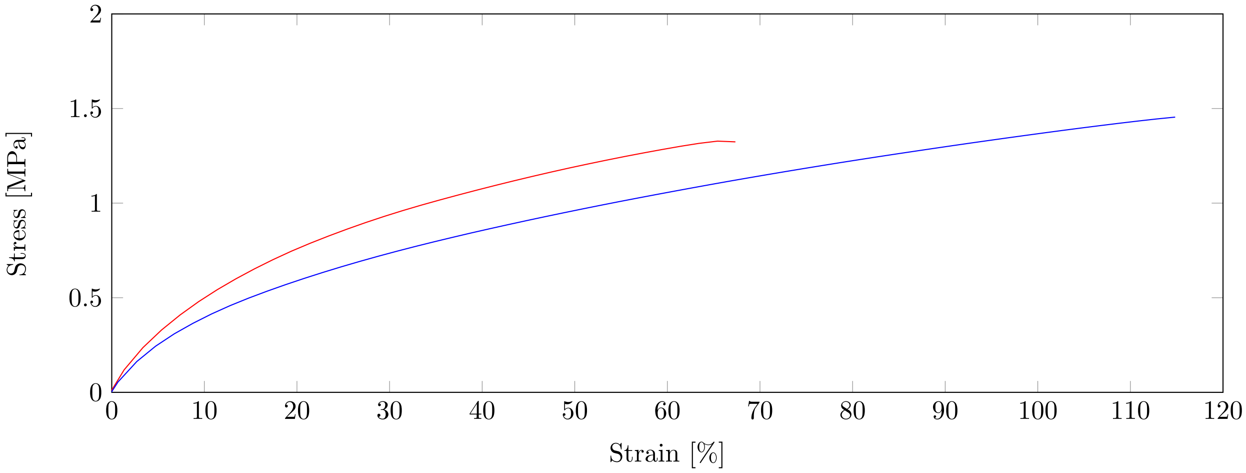

Figure D.2: Stress-strain curves of printed samples JT5000 in the 90 ° direction. Two samples were tested at a strain rate of 60 %/min at an ambient temperature of 25 °C. The ultimate tensile strength is 1.4±0.1 MPa at a strain of 91±34 %. The Young's modulus is 5.3±1.0 MPa.

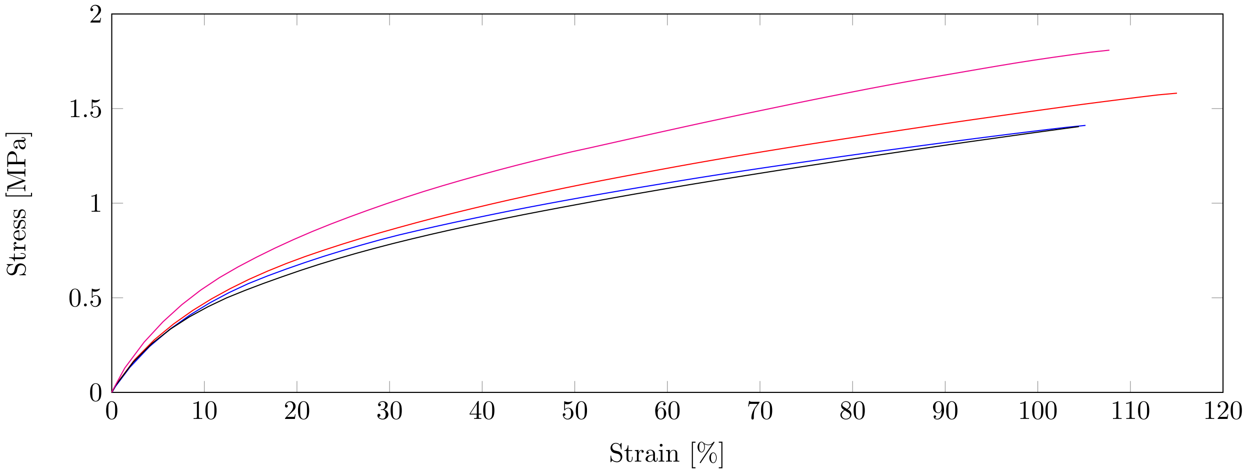

Figure D.3: Stress-strain curves of printed samples JT5000 in the ±45 ° alternating directions. Four samples were tested at a strain rate of 60 %/min at an ambient temperature of 25 °C. The ultimate tensile strength is 1.6±0.2 MPa at a strain of 108±5 %. The Young's modulus is 6.2±0.6 MPa.

Appendix E

Stress-strain curves of joined samples JT5000-JD4000

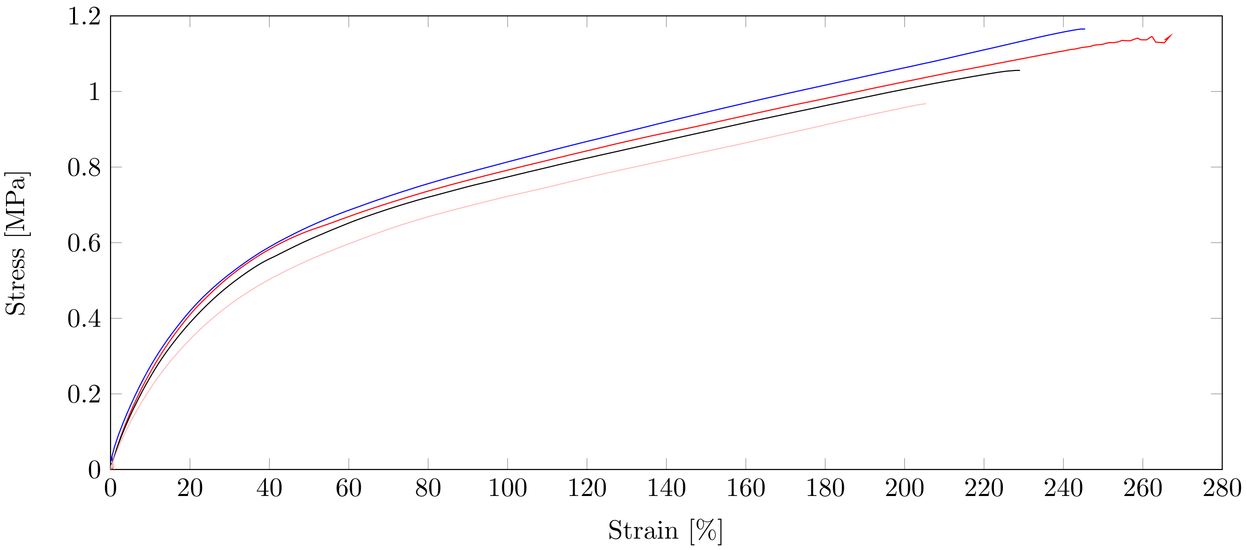

Figure E.1: Stress-strain curves of samples JD4000 and JT5000 healed to each other for 60 min at 90 °C. Four samples were tested at a strain rate of 60%/min at an ambient temperature of 25 °C with open furnace. The ultimate tensile strength is 1.1±0.1 MPa at a fracture strain of 237±26 %.

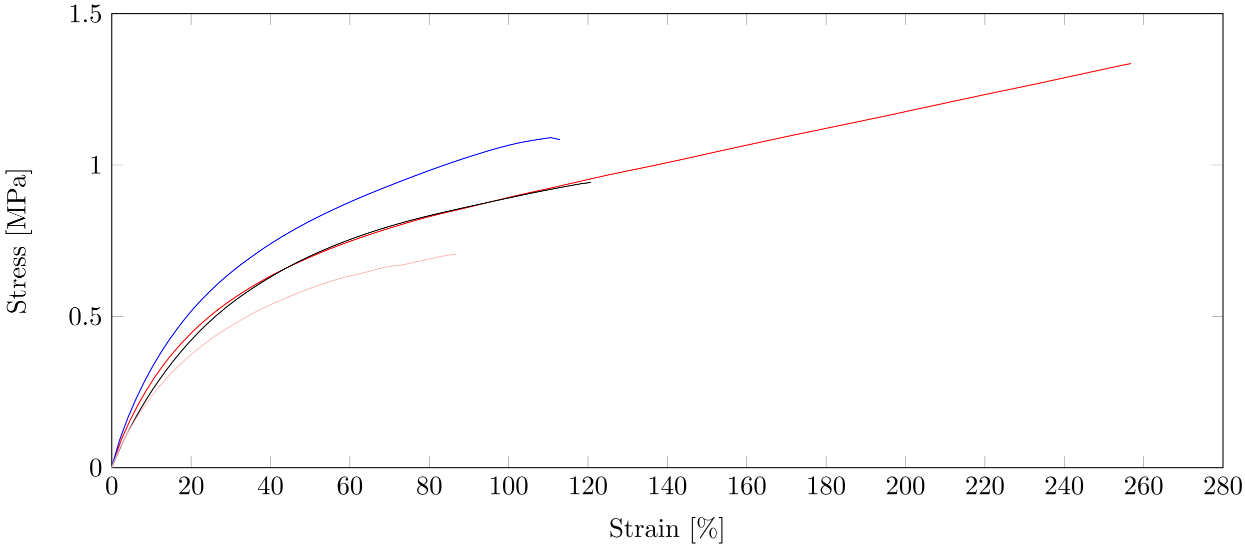

Figure E.2: Stress-strain curves of samples JD4000 and JT5000 healed to each other for 60 min at 80 °C. Four samples were tested at a strain rate of 60%/min at an ambient temperature of 25 °C with open furnace. The ultimate tensile strength is 1.0±0.3 MPa at a fracture strain of 144±76 %.

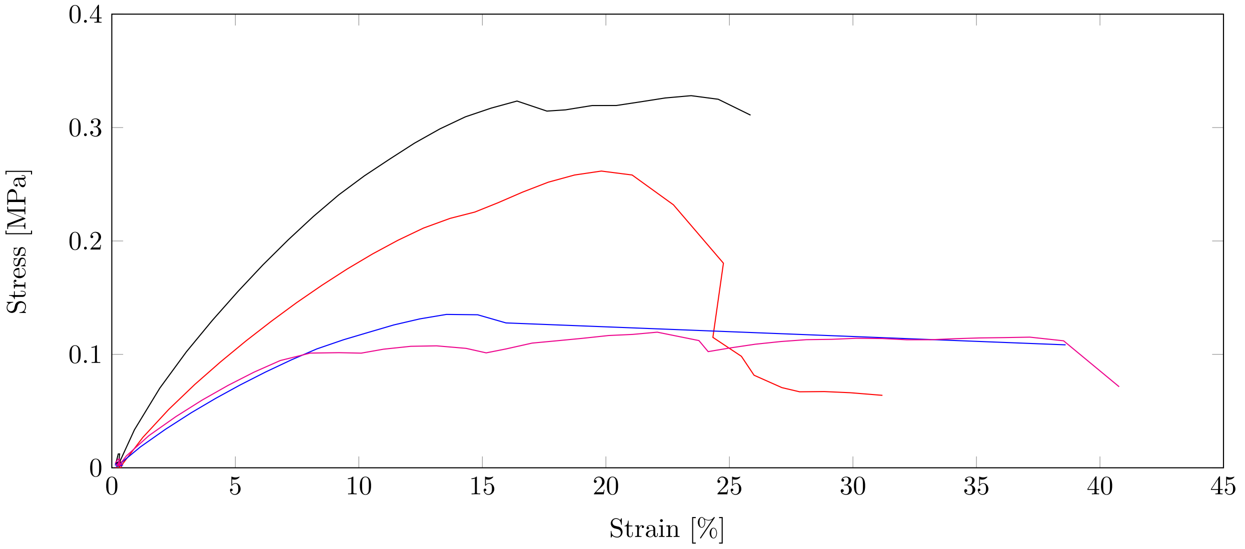

Figure E.3: Stress-strain curves of samples JD4000 and JT5000 glued to each other. Four samples were tested at a strain rate of 60%/min at an ambient temperature of 25 °C with open furnace. The ultimate tensile strength is 0.3±0.1 MPa at a strain of 43±24 %.

Bibliography

[1] S. Terryn, J. Brancart, D. Lefeber, G. Van Assche, and B. Vanderborght, "Self-healing soft pneumatic robots," *Science Robotics*, vol. 2, no. 9, 2017.

[2] S. Terryn, J. Brancart, D. Lefeber, G. V. Assche, and B. Vanderborght, "A pneumatic artificial muscle manufactured out of self-healing polymers that can repair macroscopic damages," *IEEE Robotics and Automation Letters*, vol. 3, no. 1, pp. 16–21, Jan 2018.

[3] B. Gorissen, D. Reynaerts, S. Konishi, K. Yoshida, J.-W. Kim, and M. De Volder, "Elastic inflatable actuators for soft robotic applications," *Advanced Materials*, pp. 1 604 977–n/a, 2017.

[4] B. Vanderborght, A. Albu-Schaeffer, A. Bicchi, E. Burdet, D. Caldwell, R. Carloni, M. Catalano, O. Eiberger, W. Friedl, G. Ganesh, M. Garabini, M. Grebenstein, G. Grioli, S. Haddadin, H. Hoppner, A. Jafari, M. Laffranchi, D. Lefeber, F. Petit, S. Stramigioli, N. Tsagarakis, M. V. Damme, R. V. Ham, L. Visser, and S. Wolf, "Variable impedance actuators: A review," *Robotics and Autonomous Systems*, vol. 61, no. 12, pp. 1601 – 1614, 2013.

[5] D. Trivedi, C. D. Rahn, W. M. Kier, and I. D. Walker, "Soft robotics: Biological inspiration, state of the art, and future research," *Applied Bionics and Biomechanics*, vol. 5, no. 3, pp. 99–117, 2008.

[6] S. Kim, C. Laschi, and B. Trimmer, "Soft robotics: a bioinspired evolution in robotics," *Trends in Biotechnology*, vol. 31, no. 5, pp. 287 – 294, 2013.

[7] D. Rus and M. T. Tolley, "Design, fabrication and control of soft robots," *Nature*, vol. 521, no. 7553, p. 467, 2015.

[8] R. Bogue, "Flexible and soft robotic grippers: the key to new markets?" *Industrial Robot: An International Journal*, vol. 43, no. 3, pp. 258–263, 2016.

[9] M. E. Giannaccini, I. Georgilas, I. Horsfield, B. Peiris, A. Lenz, A. G. Pipe, and S. Dogramadzi, "A variable compliance, soft gripper," *Autonomous Robots*, vol. 36, no. 1-2, pp. 93–107, 2013.

[10] M. Manti, T. Hassan, G. Passetti, N. D'Elia, C. Laschi, and M. Cianchetti, "A bioinspired soft robotic gripper for adaptable and effective grasping," *Soft Robotics*, vol. 2, no. 3, pp. 107–116, 2015.

[11] D. Villegas, M. V. Damme, B. Vanderborght, P. Beyl, and D. Lefeber, "Third–generation pleated pneumatic artificial muscles for robotic applications: Development and comparison with mckibben muscle," *Advanced Robotics*, vol. 26, no. 11-12, pp. 1205–1227, 2012.

[12] S. Terryn, G. Mathijssen, J. Brancart, T. Verstraten, G. V. Assche, and B. Vanderborght, “Toward self-healing actuators: A preliminary concept,” *IEEE Transactions on Robotics*, vol. 32, no. 3, pp. 736–743, June 2016.

[13] C. Blanes, M. Mellado, and P. Beltran, “Novel additive manufacturing pneumatic actuators and mechanisms for food handling grippers,” in *Actuators*, vol. 3, no. 3. Multidisciplinary Digital Publishing Institute, 2014, pp. 205–225.

[14] M. D. Hager, P. Greil, C. Leyens, S. van der Zwaag, and U. S. Schubert, “Self-healing materials,” *Advanced Materials*, vol. 22, no. 47, pp. 5424–5430, 2010.

[15] S. R White, N. Sottos, P. Geubelle, J. Moore, M. R Kessler, S. Sriram, E. Brown, and S. Viswanathan, “Autonomic healing of polymer composites,” *Nature*, vol. 409, pp. 794–7, 03 2001.

[16] N. M. corporation, “Scratch shield,” http://www.nissan-global.com/EN/TECHNOLOGY/OVERVIEW/scratch.html, accessed: 06/08/2017.

[17] LG, “Back cover self-healing technology,” http://www.lg.com/ca_en/support/product-help/CT20098088-1434701085113-broken-part-accessory, accessed: 16/10/2017.

[18] N. K. Guimard, K. K. Oehlenschlaeger, J. Zhou, S. Hilf, F. G. Schmidt, and C. Barner-Kowollik, “Current trends in the field of self-healing materials,” *Macromolecular Chemistry and Physics*, vol. 213, no. 2, pp. 131–143, 2012.

[19] N. G. Cheng, A. Gopinath, L. Wang, K. Iagnemma, and A. E. Hosoi, “Thermally tunable, self-healing composites for soft robotic applications,” *Macromolecular Materials and Engineering*, vol. 299, no. 11, pp. 1279–1284, 2014.

[20] S. C. Ligon, R. Liska, J. Stampfl, M. Gurr, and R. Mülhaupt, “Polymers for 3d printing and customized additive manufacturing,” *Chemical Reviews*, vol. 117, no. 15, pp. 10 212–10 290, 2017.

[21] H. Lipson and M. Kurman, *Fabricated: The new world of 3D printing.* John Wiley & Sons, 2013.

[22] M. Sljivic, A. Pavlovic, J. Ilić, and M. Stanojevic, *Sustainable Small Batch Reproduction via Additive Manufacturing and Vacuum Casting: The Case Study of a Rhinoceros Toy Figure.* Cham: Springer International Publishing, 2017, pp. 713–722.

[23] S. Crump, “Apparatus and method for creating three-dimensional objects,” US Patent US5 121 329 A, Jun. 9, 1992.

[24] A. Södergård and M. Stolt, “Properties of lactic acid based polymers and their correlation with composition,” *Progress in Polymer Science*, vol. 27, no. 6, pp. 1123 – 1163, 2002.

[25] A. Zolfagharian, A. Z. Kouzani, S. Y. Khoo, A. A. A. Moghadam, I. Gibson, and A. Kaynak, “Evolution of 3d printed soft actuators,” *Sensors and Actuators A: Physical*, vol. 250, pp. 258 – 272, 2016.

[26] Y. She, C. Li, J. Cleary, and H.-J. Su, “Design and fabrication of a soft robotic hand with embedded actuators and sensors,” *Journal of Mechanisms and Robotics*, vol. 7, no. 2, p. 021007, 2015.

[27] L. Stiltner, A. Elliott, and C. Williams, "A method for creating actuated joints via fiber embedding in a polyjet 3d printing process," vol. 22, pp. 583–592, 01 2011.

[28] T. Umedachi, V. Vikas, and B. A. Trimmer, "Highly deformable 3-d printed soft robot generating inching and crawling locomotions with variable friction legs," in *IEEE/RSJ International Conference on Intelligent Robots and Systems (IROS).* IEEE, 2013, pp. 4590–4595.

[29] B. N. Peele, T. J. Wallin, H. Zhao, and R. F. Shepherd, "3d printing antagonistic systems of artificial muscle using projection stereolithography," *Bioinspiration & Biomimetics*, vol. 10, no. 5, p. 055003, 2015.

[30] H. K. Yap, H. Y. Ng, and C.-H. Yeow, "High-force soft printable pneumatics for soft robotic applications," *Soft Robotics*, vol. 3, no. 3, pp. 144–158, 2016.

[31] B. Trimmer, J. Lewis, R. F. Shepherd, and H. Lipson, "3d printing soft materials: What is possible?" 2015.

[32] N. W. Bartlett, M. T. Tolley, J. T. Overvelde, J. C. Weaver, B. Mosadegh, K. Bertoldi, G. M. Whitesides, and R. J. Wood, "A 3d-printed, functionally graded soft robot powered by combustion," *Science*, vol. 349, no. 6244, pp. 161–165, 2015.

[33] M. Wehner, R. L. Truby, D. J. Fitzgerald, B. Mosadegh, G. M. Whitesides, J. A. Lewis, and R. J. Wood, "An integrated design and fabrication strategy for entirely soft, autonomous robots," *Nature*, vol. 536, no. 7617, p. 451, 2016.

[34] M. Zarek, M. Layani, I. Cooperstein, E. Sachyani, D. Cohn, and S. Magdassi, "3d printing of shape memory polymers for flexible electronic devices," *Advanced Materials*, vol. 28, no. 22, pp. 4449–4454, 2016.

[35] Y. Yang, Y. Chen, Y. Wei, and Y. Li, "3d printing of shape memory polymer for functional part fabrication," *The International Journal of Advanced Manufacturing Technology*, vol. 84, no. 9, pp. 2079–2095, Jun 2016.

[36] M. Nadgorny, Z. Xiao, and L. A. Connal, "2d and 3d-printing of self-healing gels: design and extrusion of self-rolling objects," *Molecular Systems Design and Engineering*, vol. 2, pp. 283–292, 2017.

[37] S. Terryn, G. Mathijssen, J. Brancart, D. Lefeber, G. Van Assche, and B. Vanderborght, "Development of a self-healing soft pneumatic actuator: A first concept," *Bioinspiration & biomimetics*, vol. 10, no. 4, p. 046007, 2015.

[38] H. H. Winter and F. Chambon, "Analysis of linear viscoelasticity of a crosslinking polymer at the gel point," *Journal of rheology*, vol. 30, no. 2, pp. 367–382, 1986.

[39] A. Cuvellier, R. Verhelle, J. Brancart, B. Vanderborght, G. Van Assche, and H. Rahier, "The influence of stereochemistry on the reactivity of the diels-alder cycloaddition and the implications for reversible network polymerization," *Submitted for peer review*, 2018.

[40] D. V. Rosato, *Extruding plastics: a practical processing handbook.* Springer Science & Business Media, 2013.

[41] R. J. Koopmans and J. Molenaar, "The "sharkskin effect" in polymer extrusion," *Polymer Engineering & Science*, vol. 38, no. 1, pp. 101–107, 1998.

[42] B. Meulenbroek, C. Storm, V. Bertola, C. Wagner, D. Bonn, and W. van Saarloos, “Intrinsic route to melt fracture in polymer extrusion: A weakly nonlinear subcritical instability of viscoelastic poiseuille flow,” *Physical Review Letters*, vol. 90, p. 024502, Jan 2003.

[43] N. E. Kissi, J.-M. Piau, and F. Toussaint, “Sharkskin and cracking of polymer melt extrudates,” *Journal of Non-Newtonian Fluid Mechanics*, vol. 68, no. 2, pp. 271 – 290, 1997, papers presented at the Polymer Melt Rheology Conference.

[44] J.-F. Agassant, D. R. Arda, C. Combeaud, A. Merten, H. Muenstedt, M. R. Mackley, L. Robert, and B. Vergnes, “Polymer processing extrusion instabilities and methods for their elimination or minimisation,” *International Polymer Processing*, vol. 21, no. 3, pp. 239–255, 2006.

[45] *NinjaFlex® 3D Printing Filament - Technical specifications*, NinjaTek, 2016. [Online]. Available: https://ninjatek.com/wp-content/uploads/2016/05/NinjaFlex-TDS.pdf

[46] M. Ko, H. Kang, J. ulrim Kim, Y. Lee, and J.-E. Hwang, “How to measure quality of affordable 3d printing: Cultivating quantitative index in the user community,” in *International Conference on Human-Computer Interaction.* Springer, 2016, pp. 116–121.

[47] R. Zou, Y. Xia, S. Liu, P. Hu, W. Hou, Q. Hu, and C. Shan, “Isotropic and anisotropic elasticity and yielding of 3d printed material,” *Composites Part B: Engineering*, vol. 99, pp. 506 – 513, 2016.